Time-Domain Electromagnetic Fields Radiating Along the Horizontal Interface Between Vertically Uniaxial Half-Space Media

Won-seok Lihh, *Member, IEEE*, and Sangwook Nam, *Member, IEEE*

***Abstract*—At the horizontal interface between vertically uniaxial half-space media, the propagation of electromagnetic fields is theoretically investigated for an interfacial impulse current source of infinitesimal size. For the electric field, the problem divides into the horizontal source and horizontal receiver (HH), vertical source and vertical receiver (VV), horizontal source and vertical receiver (HV), and vertical source and horizontal receiver (VH) cases. Employing the interface scheme of the Cagniard-style analysis, the solutions of the HH and VV cases are obtained in exact explicit forms. The solutions of the HV and VH cases cannot be expressed in integral-free forms, but the impulse components implicit in the integral solutions can be analytically extracted without the aid of the frequency-domain asymptotic techniques. Investigation is also made of the magnetic field and of the variation of waveforms when the receiver is taken a little off the interface. The uniaxial case is a generalization of the isotropic case, affording richer information of the wave physics.**

***Index Terms*—Anisotropic media, dielectric interfaces, electromagnetic transient propagation, time-domain analysis.**

I. Introduction

THE wave reflection at a planar interface has been a classical topic of continued interest in the time-domain analysis of stratified structures. Depending on the physical aspect of the media, the wavefields can be electromagnetic [1, Sec. 5.5], [2, Ch. 4], [3]–[5] or acoustic/elastic [6, Ch. 6], [7]–[10]. The case in which the wave source is placed exactly at or infinitesimally close to the interface is a special case of the reflection problem. For a time-harmonic interfacial dipole, in the electromagnetic case, the spherical space wave has a far-field null along the interface [11], [12].

To obtain the dominant fields near the interface null, one can perform an asymptotic analysis for the lateral-wave components (of the head-wave type or not) contributed by the branch-line integrals in the wavenumber (or complex angle) domain [1, Sec. 5.5], [2, Sec. 2.6.1], [13]. The time-domain fields at the interface are then approximated by the transient counterparts of the lateral-wave components. For more detailed description at the interface, however, the branch-line integrals need to be analyzed more thoroughly, being directly evaluated in terms of elementary functions if possible. The simplest case of the transient electromagnetic fields is the one for lossless isotropic media [4], [14]–[17].

To be studied in this paper is the interface problem for uniaxially anisotropic media. The upper and lower half-space media are lossless and uniaxial with the symmetry axis normal to the horizontal interface. More generalized solutions are obtained than in the isotropic case, since the uniaxiality imposes different wavespeeds on the "tangential-electric" (TE) and "tangential-magnetic" (TM) waves at the interface. The horizontal source generates both the TE and TM waves, while the vertical source generates the TM wave only. The uniaxial case reveals the dependence of a field on the horizontal and vertical permittivities. Either of the media or both can be made isotropic by setting these permittivities equal. For detailed knowledge of the wave propagation, the authors are concerned with the electric (E) and magnetic (H) fields rather than the modal or potential Green's functions.

Among the various analytical studies [4], [10], [14]–[19], the authors adopt the scheme of [16], which can be regarded as an interface version of the Cagniard's method [20] or de Hoop's later modification [21]. De Hoop's approach is free from the catalytic use of the special functions such as the Hankel and modified Bessel functions; hence it might appear that the special functions used in this paper are redundant. However, the authors will not avoid using them, in order to see the formulational similarity and difference between the horizontal source and horizontal receiver (HH) and vertical source and vertical receiver (VV) cases on the one hand and the horizontal source and vertical receiver (HV) and vertical source and horizontal receiver (VH) cases on the other. In addition, the authors will use the wavenumbers (as the transform variables) rather than the slowness or angle parameters, for better compatibility with the spatial differentiations.

The E fields are solved in exact explicit forms for the HH and VV cases, while remaining in single-integral forms for the HV and VH cases. Even in the HV and VH cases, the impulse component implicit in an integral solution can be analytically extracted as the early-time singularity, without the aid of the asymptotic analysis in the frequency domain (though there may be some equivalence). The impulse components are worthwhile in their own right as conspicuous singularities in the time-domain waveforms, whether or not in the far zone. The H fields can be obtained by adapting the procedures for the E fields. There is no need to express the solutions in different forms depending on the relative values of horizontal and vertical permittivities (of the upper and lower media). This is an improvement

Manuscript received July 20, 2006; revised December 5, 2006.

W. Lihh is with Global Communication Technology (GCT) Research, Inc., Seoul, Korea (e-mail: wslee@gctsemi.com).

S. Nam is with the School of Electrical Engineering, Seoul National University, Seoul, Korea (e-mail: snam@snu.ac.kr).

Digital Object Identifier 10.1109/TAP.2007.895623

0018-926X/$25.00 © 2007 IEEE

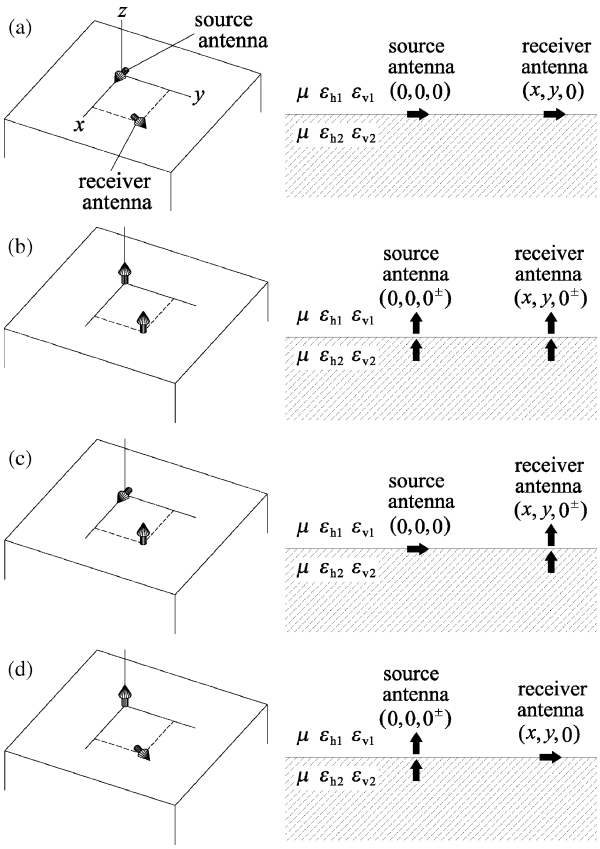

Fig. 1. The interface problem for vertically uniaxial media: (a) the HH case; (b) the VV case; (c) the HV case; and (d) the VH case. The horizontal source can be assumed to be x-directional without loss of generality.

on the previous acoustical analyses [8], [10] in which the interface solutions are derived casewise depending on the values of the wavespeeds in the fluid media (for a given density ratio).

The interface solutions are solved in Section III, and there follows a section discussing the relation between the leading impulse components of the interface solutions and the lateral head waves (Section IV). The Poynting vectors determined by the leading impulse components make critical angles with the vertical axis. Due to the uniaxiality, the critical angle of the TM wave is not equal to that of the TE wave. Section V discusses the deformation of waveforms when the receiver is taken a little off the interface, in connection with the spherical space waves, the head waves, and the unguided surface waves.

II. Maxwell's Equations in Fourier–Laplace (FL) Domain

The configurations of the interface problem are shown in Fig. 1, where the source and receiver antennas are located exactly at the interface or infinitesimally above or infinitesimally below. The upper and lower media are uniaxially anisotropic with positive real permittivities in the horizontal and vertical directions: $\varepsilon_{\rm h1}$, $\varepsilon_{\rm h2}$, $\varepsilon_{\rm v1}$, and $\varepsilon_{\rm v2}$. The permeability μ is assumed to be the free-space one (μ_0). Although the cases $\varepsilon_{\rm h1} = \varepsilon_{\rm h2}$, $\varepsilon_{\rm v1} = \varepsilon_{\rm v2}$, and $\varepsilon_{\rm h1}\varepsilon_{\rm v1} = \varepsilon_{\rm h2}\varepsilon_{\rm v2}$ make some denominator(s) zero in the formulation, the analysis in this paper does not lose its validity. These special cases can be handled by taking the relevant limit(s) in the final expressions of the fields, or, more preferably, by analogously applying the procedures in this paper from the beginning.

A classical way of analysis is via the FL transformation and the Cagniard inversion into the physical (space and time) domain [6, p. 190]. The Fourier plane transform $\mathcal{P}$ and the Laplace time transform $\mathcal{L}$ are applied to the Maxwell's curl equations $\boldsymbol{\nabla}\times\mathbf{E} = -\mu\,\partial_t\mathbf{H}$ and $\boldsymbol{\nabla}\times\mathbf{H} = \mathbf{J} + [(\mathbf{i}_x\mathbf{i}_x + \mathbf{i}_y\mathbf{i}_y)\varepsilon_{\rm h} + \mathbf{i}_z\mathbf{i}_z\,\varepsilon_{\rm v}]\cdot\partial_t\mathbf{E}$, assuming initial quiescence. The conventions $\mathcal{P}\{(\partial_x, \partial_y)\} = -j(k_x, k_y)$ and $\mathcal{L}\{\partial_t\} = s$ are adopted, where s is real and positive. In the FL domain is introduced the α-rotation which relates the x- and y-directional components of a vector field, say $\mathring{\mathbf{F}}$ $(= \mathcal{LP}\{\mathbf{F}\})$, to the k- and α-directional ones

$$\begin{pmatrix} \mathring{F}_k \\ \mathring{F}_\alpha \end{pmatrix} = \begin{pmatrix} \cos\alpha & \sin\alpha \\ -\sin\alpha & \cos\alpha \end{pmatrix} \begin{pmatrix} \mathring{F}_x \\ \mathring{F}_y \end{pmatrix} \tag{1}$$

where $(\cos\alpha, \sin\alpha) = (k_x, k_y)/k$ with $k = (k_x^2 + k_y^2)^{1/2}$. By the composite transform $\mathcal{LP}$ $(\triangleq \mathcal{C})$ and the α-rotation, the curl equations are decomposed into the TE wave equations

$$\partial_z \mathring{E}_\alpha = s\mu \mathring{H}_k \tag{2}$$

$$\partial_z \mathring{H}_k = \frac{\gamma_{\rm h}^2}{s\mu}\mathring{E}_\alpha + \mathring{J}_\alpha \tag{3}$$

$$\mathring{H}_z = \frac{jk}{s\mu}\mathring{E}_\alpha \tag{4}$$

and the TM wave equations

$$\partial_z \mathring{E}_k = -\frac{\gamma_{\rm v}^2}{s\,\varepsilon_{\rm v}}\mathring{H}_\alpha + \frac{jk}{s\,\varepsilon_{\rm v}}\mathring{J}_z \tag{5}$$

$$\partial_z \mathring{H}_\alpha = -s\,\varepsilon_{\rm h}\,\mathring{E}_k - \mathring{J}_k \tag{6}$$

$$\mathring{E}_z = -\frac{jk}{s\,\varepsilon_{\rm v}}\mathring{H}_\alpha - \frac{1}{s\,\varepsilon_{\rm v}}\mathring{J}_z \tag{7}$$

where $\varepsilon_{\rm (h,v)} = \varepsilon_{\rm (h,v)n}$ and

$$\gamma_{\rm (h,v)} = \gamma_{\rm (h,v)n} = \left(k^2 + s^2 c_{\rm (h,v)n}^{-2}\right)^{1/2}$$

in the medium n $(\in \{1, 2\})$, with $c_{\rm (h,v)n} = (\mu\,\varepsilon_{\rm (h,v)n})^{-1/2}$. The wave solutions in the FL domain (and their counterparts in the physical domain) are referred to as the TE and TM waves, which can also be called the ordinary and extraordinary waves, respectively. The z-directional wavenumber of the TM wave is not $\gamma_{\rm vn}$ but $\chi_n\gamma_{\rm vn}$ (where χ_n is the anisotropy ratio $(\varepsilon_{\rm hn}/\varepsilon_{\rm vn})^{1/2}$), while the wavenumber of the TE wave is $\gamma_{\rm hn}$, as can be noticed from (5) and (6) for the former and from (2) and (3) for the latter.

III. Derivation of Interfacial Fields in Physical Domain

Let the current source be excited by a Dirac signal $\delta(t)$. In the HH and HV cases, the horizontal source can be assumed to be x-directional without loss of generality. The horizontal source can be assumed to be located exactly at

the interface, because its slight superjacency/subjacency does not affect the amounts of excited fields. Hence, for the HH and HV cases, one can assign $\mathbf{J} = \mathbf{i}_x\delta(\boldsymbol{\rho})\delta(z)\delta(t)$ [dropping the formal unity factor 1 coulomb meter (C m)], where $\boldsymbol{\rho} = \mathbf{i}_x\, x + \mathbf{i}_y\, y$ and $\delta(\boldsymbol{\rho}) = \delta(x)\delta(y)$. Or, in the FL domain, $\mathring{\mathbf{J}} = (\mathbf{i}_k\cos\alpha - \mathbf{i}_\alpha\sin\alpha)\delta(z)$. A vertical source generates different amounts of fields depending on whether it is located above or below the interface. The fields of the subjacent source are the $(\varepsilon_{\mathrm{v}1}/\varepsilon_{\mathrm{v}2})$-scaled versions of those of the superjacent source [see the last terms of (5) and (7)]. Hence, just let $\mathbf{J} = \mathbf{i}_z\delta(\boldsymbol{\rho})\delta(z-0^+)\delta(t)$ for the VV and VH cases; or, in the FL domain, $\mathring{\mathbf{J}} = \mathbf{i}_z\delta(z-0^+)$.

A. The HH Case

In the HH case [Fig. 1(a)], the E fields of interest are the x- and y-directional ones. Solving (2) and (3) with $\mathring{J}_\alpha = -\delta(z)\sin\alpha$ and solving (5) and (6) with $\mathring{J}_k = \delta(z)\cos\alpha$ (and $\mathring{J}_z = 0$), one can obtain the modal E fields at $z = 0$ as

$$\mathring{E}_{\alpha//\alpha//} = \frac{-Z_1^{\mathrm{TE}}Z_2^{\mathrm{TE}}}{Z_1^{\mathrm{TE}} + Z_2^{\mathrm{TE}}} = \frac{-s\mu}{\gamma_{\mathrm{h}1} + \gamma_{\mathrm{h}2}} \tag{8}$$

$$\mathring{E}_{k//k//} = \frac{-Z_1^{\mathrm{TM}}Z_2^{\mathrm{TM}}}{Z_1^{\mathrm{TM}} + Z_2^{\mathrm{TM}}} = \frac{-V_1V_2}{s(V_1 + V_2)} \tag{9}$$

where $Z_n^{\mathrm{TE}} = s\mu/\gamma_{\mathrm{h}n}$ and $Z_n^{\mathrm{TM}} = V_n/s$ with $V_n = \gamma_{\mathrm{v}n}/\dot{\varepsilon}_n$; here $\dot{\varepsilon}_n = (\varepsilon_{\mathrm{h}n}\,\varepsilon_{\mathrm{v}n})^{1/2}$. The notation $\mathring{E}_{pq}$ represents the p-directional E field (in the FL domain) generated by the q-directional source. The mark // indicates that the field under consideration is not affected by the infinitesimal offset of the source (or the receiver) from the interface. By (1), one can write

$$\begin{pmatrix} \mathring{E}_{x//x//}^{\mathrm{TE}} \\ \mathring{E}_{y//x//}^{\mathrm{TE}} \end{pmatrix} = \begin{pmatrix} \sin^2\alpha \\ -\cos\alpha\sin\alpha \end{pmatrix} \mathring{E}_{\alpha//\alpha//} \tag{10}$$

$$\begin{pmatrix} \mathring{E}_{x//x//}^{\mathrm{TM}} \\ \mathring{E}_{y//x//}^{\mathrm{TM}} \end{pmatrix} = \begin{pmatrix} \cos^2\alpha \\ \cos\alpha\sin\alpha \end{pmatrix} \mathring{E}_{k//k//}. \tag{11}$$

Adding (10) and (11) gives the full horizontal fields.

First, consider $\mathring{E}_{x//x//}^{\mathrm{TE}}$ $(= \mathring{E}_{\alpha//\alpha//}\sin^2\alpha)$, of which the physical domain counterpart can be written as

$$E_{x//x//}^{\mathrm{TE}} = \frac{-\partial_y^2}{\varepsilon_{\mathrm{h}2} - \varepsilon_{\mathrm{h}1}} \mathcal{L}^{\mathrm{i}}\mathcal{B}^{\mathrm{i}}\Big\{\frac{\gamma_{\mathrm{h}1}}{sk^2} - \frac{\gamma_{\mathrm{h}2}}{sk^2}\Big\}. \tag{12}$$

The superscript i indicates the inverse transform. The operator $\mathcal{B}^{\mathrm{i}}$ is a variant of $\mathcal{P}^{\mathrm{i}}$, acting on an α-independent operand

$$\begin{aligned} \mathcal{B}^{\mathrm{i}}\{G(k)\} &= \frac{1}{4\pi}\int_{C_k} G(k)\, H_0^{(2)}(k\rho)\, k\,\mathrm{d}k \\ &= \frac{-js^2}{2\pi^2\rho^2}\int_{C_\tau} G\Big(-j\frac{s\tau}{\rho}\Big) K_0(s\tau)\,\tau\,\mathrm{d}\tau \end{aligned} \tag{13}$$

where $\rho = |\boldsymbol{\rho}| = (x^2 + y^2)^{1/2}$ and where $K_0(s\tau) = -j(\pi/2)H_0^{(2)}(-js\tau)$ for $\arg\tau \in (-\pi/2, \pi)$ [22, p. 375]. Here $H_0^{(2)}(\,)$ and $K_0(\,)$ are the Hankel and modified Bessel functions, respectively, both being of the second kind and of order zero. The integration contours C_k and C_τ are the "Cagniard paths" in the complex k and τ planes, respectively.

For $G(k) = \gamma_{\mathrm{h}n}/(sk^2)$ in (12) $(n \in \{1, 2\})$, one can write $G(-js\tau/\rho) = -(\rho\,\hat{\tau}_{\mathrm{h}n})/(s^2\tau^2)$ where $\hat{\tau}_{\mathrm{h}n} = (c_{\mathrm{h}n}^{-2}\rho^2 - \tau^2)^{1/2}$. The path C_τ in this case is shown in Fig. 2. This kind of path,

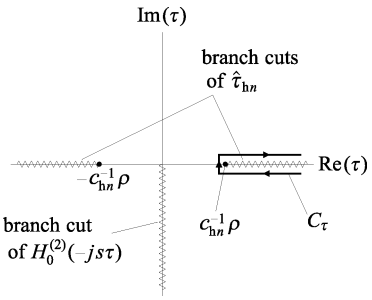

Fig. 2. The integration path C_τ for $G(-js\tau/\rho) = -(\rho\,\hat{\tau}_{\mathrm{h}n})/(s^2\tau^2)$.

without the (horned) hyperbolic shape typical of a reflection/transmission problem, is specific to the interface problem [16], [23]. Now one can write

$$\mathcal{B}^{\mathrm{i}}\Big\{\frac{\gamma_{\mathrm{h}n}}{sk^2}\Big\} = \frac{1}{\pi^2\rho}\int_{c_{\mathrm{h}n}^{-1}\rho}^{\infty} \frac{\check{\tau}_{\mathrm{h}n}}{\tau} K_0(s\tau)\,\mathrm{d}\tau \tag{14}$$

with $\check{\tau}_{\mathrm{h}n} = (\tau^2 - c_{\mathrm{h}n}^{-2}\rho^2)^{1/2}$, using the fact that $\hat{\tau}_{\mathrm{h}n} = -j\,\check{\tau}_{\mathrm{h}n}$ on C_τ in the first quadrant.

Employing the formula $\mathcal{L}^{\mathrm{i}}\{K_0(s\tau)\} = u(t-\tau)/(t^2-\tau^2)^{1/2}$ [22, p. 1028] where $u(\,)$ is the unit-step function, one can calculate the inverse Laplace transform of (14) as

$$\begin{aligned} \mathcal{L}^{\mathrm{i}}\mathcal{B}^{\mathrm{i}}\Big\{\frac{\gamma_{\mathrm{h}n}}{sk^2}\Big\} &= \frac{u(t_{\mathrm{h}n})}{\pi^2\rho}\int_{c_{\mathrm{h}n}^{-1}\rho}^{t} \frac{\check{\tau}_{\mathrm{h}n}\mathrm{d}\tau}{\tau(t^2-\tau^2)^{1/2}} \\ &= \frac{\pi}{2} I\Big(\frac{t^2}{\check{t}_{\mathrm{h}n}^2}\Big) = \frac{u(t_{\mathrm{h}n})}{2\pi}\Big(\frac{1}{\rho} - \frac{c_{\mathrm{h}n}^{-1}}{t}\Big) \end{aligned} \tag{15}$$

where $\check{t}_{\mathrm{h}n} = (t^2 - c_{\mathrm{h}n}^{-2}\rho^2)^{1/2}$ and $t_{\mathrm{h}n} = t - c_{\mathrm{h}n}^{-1}\rho$. The integration variable has been changed from τ to β through $(t^2 - \tau^2)^{1/2} = \check{t}_{\mathrm{h}n}\sin\beta$ and use has been made of

$$\begin{aligned} I(a) &\triangleq \frac{2}{\pi}\int_0^{\pi/2} \frac{\cos^2\beta\,\mathrm{d}\beta}{a - \sin^2\beta} \\ &= 1 - \Big(1 - \frac{1}{a}\Big)^{1/2} \qquad (a < 0 \text{ or } a > 1) \qquad \text{(16a)} \\ &= 1 \qquad\qquad\qquad\qquad (0 < a < 1) \qquad \text{(16b)} \end{aligned}$$

which is proven in the Appendix. The first case (16a) applies to (15), since $t^2/\check{t}_{\mathrm{h}n}^2 > 1$ for $t > c_{\mathrm{h}n}^{-1}\rho$. The second case (16b) is for later use.

Replacing ∂_y^2 in (12) with $-\partial_x\partial_y$ gives the field $E_{y//x//}^{\mathrm{TE}}$. Calculating these differentiations with (15), one can obtain the TE part of the E fields as

$$\begin{aligned} \begin{pmatrix} E_{x//x//}^{\mathrm{TE}} \\ E_{y//x//}^{\mathrm{TE}} \end{pmatrix} &= \begin{pmatrix} \frac{-y^2}{\rho^2} \\ \frac{xy}{\rho^2} \end{pmatrix} \frac{c_{\mathrm{h}1}^{-1}\delta(t_{\mathrm{h}1}) - c_{\mathrm{h}2}^{-1}\delta(t_{\mathrm{h}2})}{2\pi(\varepsilon_{\mathrm{h}2} - \varepsilon_{\mathrm{h}1})\rho^2} \\ &\quad + \begin{pmatrix} \frac{x^2-2y^2}{\rho^2} \\ \frac{3xy}{\rho^2} \end{pmatrix} \frac{u(t_{\mathrm{h}1}) - u(t_{\mathrm{h}2})}{2\pi(\varepsilon_{\mathrm{h}2} - \varepsilon_{\mathrm{h}1})\rho^3}. \end{aligned} \tag{17}$$

Here $t_{\mathrm{h}1}$ need not be larger than $t_{\mathrm{h}2}$, that is, $c_{\mathrm{h}1}^{-1}\rho$ need not be smaller than $c_{\mathrm{h}2}^{-1}\rho$. Note that

$$u(t_{\mathrm{h}1}) - u(t_{\mathrm{h}2}) = 0 \ \text{ unless } \ t \in [c_{\mathrm{h}\mathfrak{p}}^{-1}\rho, c_{\mathrm{h}\bar{\mathfrak{p}}}^{-1}\rho]$$

where $(\mathfrak{p}, \bar{\mathfrak{p}}) = (1, 2)$ if $\varepsilon_{\mathrm{h}1} < \varepsilon_{\mathrm{h}2}$ and (2, 1) if $\varepsilon_{\mathrm{h}1} > \varepsilon_{\mathrm{h}2}$.

Next, consider $\mathring{E}^{\mathrm{TM}}_{x/\!/x/\!/}$ $(=\mathring{E}_{k/\!/k/\!/}\cos^2\alpha)$, of which the physical domain counterpart is expanded as

$$E^{\mathrm{TM}}_{x/\!/x/\!/} = \mathcal{C}^{\mathrm{i}}\left\{-\frac{k_x^2(V_1V_2^2 - V_1^2V_2)}{sk^2(V_2^2 - V_1^2)}\right\} = \sum_{n=1}^{2}\frac{-\dot{\varepsilon}_n\partial_x^2}{\dot{\varepsilon}_{\bar{n}}^2 - \dot{\varepsilon}_n^2}\mathcal{C}^{\mathrm{i}}\left\{\frac{\frac{\gamma_{\mathrm{v}n}\gamma_{\mathrm{v}\bar{n}}^2}{(sk^2)}}{k^2 + s^2Q}\right\} \tag{18}$$

where $Q = (\dot{\varepsilon}_2^2 c_{\mathrm{v}1}^{-2} - \dot{\varepsilon}_1^2 c_{\mathrm{v}2}^{-2})/(\dot{\varepsilon}_2^2 - \dot{\varepsilon}_1^2)$. By the procedure that leads to (14), the $\mathcal{C}^{\mathrm{i}}\{\ \}$ part under summation becomes

$$\mathcal{L}^{\mathrm{i}}\left\{\frac{1}{\pi^2\rho}\left(\int_{c_{\mathrm{v}n}^{-1}\rho}^{\infty}\right)\frac{\check{\tau}_{\mathrm{v}n}\check{\tau}_{\mathrm{v}\bar{n}}^2}{\tau\,\Psi(\tau)}K_0(s\tau)\,\mathrm{d}\tau\right\} \tag{19}$$

where $\check{\tau}_{\mathrm{v}(n,\bar{n})} = (\tau^2 - c_{\mathrm{v}(n,\bar{n})}^{-2}\rho^2)^{1/2}$ and $\Psi(\tau) = \tau^2 - Q\rho^2$. The indices n and $\bar{n}$ are complementarily assigned; that is, $(n,\bar{n}) = (1,2)$ or $(2,1)$. When $Q > c_{\mathrm{v}n}^{-2}$, the function $\Psi(\tau)$ is zero at the (Sommerfeld) pole $\tau = Q^{1/2}\rho$, around which the τ integration has to be detoured from the real axis. However, there is no need to take into account the residues of the pole, since they cancel out in (18). Only the Cauchy principal value counts.

Changing the integration variable by $(t^2 - \tau^2)^{1/2} = \check{t}_{\mathrm{v}n}\sin\beta$ with $\check{t}_{\mathrm{v}n} = (t^2 - c_{\mathrm{v}n}^{-2}\rho^2)^{1/2}$, one can calculate (19) in the ordinary sense or in the principal-value sense as

$$\frac{u(t_{\mathrm{v}n})}{\pi^2\rho}\int_0^{\pi/2}\frac{\left(\frac{\check{t}_{\mathrm{v}\bar{n}}^2}{\check{t}_{\mathrm{v}n}^2} - \sin^2\beta\right)\cos^2\beta\,\mathrm{d}\beta}{\left(\frac{t^2}{\check{t}_{\mathrm{v}n}^2} - \sin^2\beta\right)\left(\frac{\Psi(t)}{\check{t}_{\mathrm{v}n}^2} - \sin^2\beta\right)} = \frac{u(t_{\mathrm{v}n})}{2\pi}\left[\frac{1}{\rho} - \frac{c_{\mathrm{v}\bar{n}}^{-2}}{Q}\frac{c_{\mathrm{v}n}^{-1}}{t} + \frac{\dot{\varepsilon}_n\dot{\varepsilon}_{\bar{n}}^2}{\Gamma Q}\frac{U(t)}{[\Gamma\Psi(t)]^{1/2}}\right] \tag{20}$$

where $t_{\mathrm{v}n} = t - c_{\mathrm{v}n}^{-1}\rho$, $\Gamma = (\dot{\varepsilon}_2^2 - \dot{\varepsilon}_1^2)/(c_{\mathrm{v}2}^{-2} - c_{\mathrm{v}1}^{-2})$, and

$$U(t) = 1 - u(-\Gamma)\,u(t - Q^{1/2}\rho).$$

The following formula has been used

$$\frac{2}{\pi}\int_0^{\pi/2}\frac{(c - \sin^2\beta)\cos^2\beta\,\mathrm{d}\beta}{(a - \sin^2\beta)(b - \sin^2\beta)} = \frac{a-c}{a-b}I(a) - \frac{b-c}{a-b}I(b) \tag{21}$$

where the function $I(\,)$ is given in (16). The product $\Gamma\Psi(t)$ in (20) is always positive for any $t\ (> c_{\mathrm{v}n}^{-1}\rho)$ that satisfies $U(t) \neq 0$, as can be reasoned from the observation

$$\begin{aligned}\Gamma > 0\ (\Leftrightarrow Q < c_{\mathrm{v}n}^{-2}) &\Longrightarrow \Psi(t) > 0\\ \Gamma < 0\ (\Leftrightarrow Q > c_{\mathrm{v}n}^{-2}) &\Longrightarrow \Psi(t) < 0 \quad (\text{for } t < Q^{1/2}\rho)\\ &\Longrightarrow \Psi(t) > 0 \quad (\text{for } t > Q^{1/2}\rho)\end{aligned}$$

for $t > c_{\mathrm{v}n}^{-1}\rho$. (Note that Γ can be written as $\dot{\varepsilon}_n^2/(c_{\mathrm{v}n}^{-2} - Q)$ for both $n = 1$ and 2.)

Replacing ∂_x^2 in (18) with $\partial_x\partial_y$ gives the field $E^{\mathrm{TM}}_{y/\!/x/\!/}$. After a straightforward but lengthy calculation for these differentiations [with (20) for the $\mathcal{C}^{\mathrm{i}}\{\ \}$ part under summation in (18)], one can obtain the TM part of the E fields as

$$\begin{aligned}\begin{pmatrix}E^{\mathrm{TM}}_{x/\!/x/\!/}\\ E^{\mathrm{TM}}_{y/\!/x/\!/}\end{pmatrix} &= \begin{pmatrix}\frac{x^2}{\rho^2}\\ \frac{xy}{\rho^2}\end{pmatrix}\frac{\eta_{\mathrm{h}1}\delta(t_{\mathrm{v}1}) + \eta_{\mathrm{h}2}\delta(t_{\mathrm{v}2})}{2\pi\rho^2}\\ &+ \begin{pmatrix}\frac{y^2 - 2x^2}{\rho^2}\\ \frac{-3xy}{\rho^2}\end{pmatrix}\frac{\dot{\varepsilon}_1 u(t_{\mathrm{v}1}) - \dot{\varepsilon}_2 u(t_{\mathrm{v}2})}{2\pi(\dot{\varepsilon}_2^2 - \dot{\varepsilon}_1^2)\rho^3}\\ &+ \begin{pmatrix}-\Psi(t) - 3\,Qx^2\\ -3\,Qxy\end{pmatrix}\frac{\dot{\varepsilon}_1^2\dot{\varepsilon}_2^2\,\Gamma\,[u(t_{\mathrm{v}1}) - u(t_{\mathrm{v}2})]}{2\pi(\dot{\varepsilon}_2^2 - \dot{\varepsilon}_1^2)[\Gamma\Psi(t)]^{5/2}}\end{aligned} \tag{22}$$

where $\eta_{\mathrm{h}n} = (\mu/\varepsilon_{\mathrm{h}n})^{1/2}$. Here $t_{\mathrm{v}1}$ need not be larger than $t_{\mathrm{v}2}$, that is, $c_{\mathrm{v}1}^{-1}\rho$ need not be smaller than $c_{\mathrm{v}2}^{-1}\rho$. Note that

$$u(t_{\mathrm{v}1}) - u(t_{\mathrm{v}2}) = 0 \ \text{ unless } \ t \in [c_{\mathrm{v}\mathfrak{q}}^{-1}\rho, c_{\mathrm{v}\bar{\mathfrak{q}}}^{-1}\rho]$$

where $(\mathfrak{q},\bar{\mathfrak{q}}) = (1,2)$ if $\varepsilon_{\mathrm{v}1} < \varepsilon_{\mathrm{v}2}$ and $(2,1)$ if $\varepsilon_{\mathrm{v}1} > \varepsilon_{\mathrm{v}2}$. It can be noticed that $\Psi(t)$ in (22) cannot be zero for $t \in [c_{\mathrm{v}\mathfrak{q}}^{-1}\rho, c_{\mathrm{v}\bar{\mathfrak{q}}}^{-1}\rho]$, since $Q\rho^2$ in $\Psi(t)$ does not lie between $c_{\mathrm{v}\mathfrak{q}}^{-2}\rho^2$ and $c_{\mathrm{v}\bar{\mathfrak{q}}}^{-2}\rho^2$. The parameter Q divides the interval $[c_{\mathrm{v}\mathfrak{q}}^{-2}, c_{\mathrm{v}\bar{\mathfrak{q}}}^{-2}]$ only externally, in the ratio $\dot{\varepsilon}_{\mathfrak{q}}^2 : \dot{\varepsilon}_{\bar{\mathfrak{q}}}^2$. In addition, $\Gamma\Psi(t)$ is positive for any $t \in [c_{\mathrm{v}\mathfrak{q}}^{-1}\rho, c_{\mathrm{v}\bar{\mathfrak{q}}}^{-1}\rho]$. Hence, the last term of (22) cannot be singular, provided that $\varepsilon_{\mathrm{v}1} \neq \varepsilon_{\mathrm{v}2}$. When $\varepsilon_{\mathrm{v}2} \to \varepsilon_{\mathrm{v}1}$, the second term on the right remains in the step function form while that last term becomes the Dirac impulse

$$\begin{pmatrix}\frac{-x^2}{\rho^2}\\ \frac{-xy}{\rho^2}\end{pmatrix}\frac{\varepsilon_{\mathrm{h}2}\eta_{\mathrm{h}1} - \varepsilon_{\mathrm{h}1}\eta_{\mathrm{h}2}}{\varepsilon_{\mathrm{h}2} - \varepsilon_{\mathrm{h}1}}\frac{\delta(t_{\mathrm{v}1})}{2\pi\rho^2}$$

derivable by considering the time integral in the interval $[c_{\mathrm{v}\mathfrak{q}}^{-1}\rho, c_{\mathrm{v}\bar{\mathfrak{q}}}^{-1}\rho]$. It is also worth noting that, when $\dot{\varepsilon}_2 \to \dot{\varepsilon}_1$ (i.e., $\varepsilon_{\mathrm{h}2}\varepsilon_{\mathrm{v}2} \to \varepsilon_{\mathrm{h}1}\varepsilon_{\mathrm{v}1}$), the sum of the second and last terms on the right-hand side of (22) does not diverge but tends to

$$\begin{aligned}&\begin{pmatrix}\frac{y^2 - 4x^2}{\rho^2}\\ \frac{-5xy}{\rho^2}\end{pmatrix}\frac{\frac{3}{2}\left(\frac{t}{\rho}\right)^2[u(t_{\mathrm{v}1}) - u(t_{\mathrm{v}2})]}{2\pi\mu\,\dot{\varepsilon}_1(\varepsilon_{\mathrm{v}2} - \varepsilon_{\mathrm{v}1})\rho^3}\\ &+ \begin{pmatrix}\frac{2x^2 - y^2}{\rho^2}\\ \frac{3xy}{\rho^2}\end{pmatrix}\frac{\left(\frac{1}{2}\varepsilon_{\mathrm{v}1} + \varepsilon_{\mathrm{v}2}\right)u(t_{\mathrm{v}1}) - \left(\varepsilon_{\mathrm{v}1} + \frac{1}{2}\varepsilon_{\mathrm{v}2}\right)u(t_{\mathrm{v}2})}{2\pi\dot{\varepsilon}_1(\varepsilon_{\mathrm{v}2} - \varepsilon_{\mathrm{v}1})\rho^3}.\end{aligned}$$

Now, adding (17) and (22) gives the final expressions for $E_{x/\!/x/\!/}$ and $E_{y/\!/x/\!/}$ as

$$\begin{aligned}\begin{pmatrix}E_{x/\!/x/\!/}\\ E_{y/\!/x/\!/}\end{pmatrix} &= \begin{pmatrix}\frac{-y^2}{\rho^2}\\ \frac{xy}{\rho^2}\end{pmatrix}\frac{\varepsilon_{\mathrm{h}1}\eta_{\mathrm{h}1}\delta(t_{\mathrm{h}1}) - \varepsilon_{\mathrm{h}2}\eta_{\mathrm{h}2}\delta(t_{\mathrm{h}2})}{2\pi(\varepsilon_{\mathrm{h}2} - \varepsilon_{\mathrm{h}1})\rho^2}\\ &+ \begin{pmatrix}\frac{x^2}{\rho^2}\\ \frac{xy}{\rho^2}\end{pmatrix}\frac{\eta_{\mathrm{h}1}\delta(t_{\mathrm{v}1}) + \eta_{\mathrm{h}2}\delta(t_{\mathrm{v}2})}{2\pi\rho^2}\\ &+ \begin{pmatrix}\frac{x^2 - 2y^2}{\rho^2}\\ \frac{3xy}{\rho^2}\end{pmatrix}\frac{u(t_{\mathrm{h}1}) - u(t_{\mathrm{h}2})}{2\pi(\varepsilon_{\mathrm{h}2} - \varepsilon_{\mathrm{h}1})\rho^3}\\ &+ \begin{pmatrix}\frac{y^2 - 2x^2}{\rho^2}\\ \frac{-3xy}{\rho^2}\end{pmatrix}\frac{\dot{\varepsilon}_1 u(t_{\mathrm{v}1}) - \dot{\varepsilon}_2 u(t_{\mathrm{v}2})}{2\pi(\dot{\varepsilon}_2^2 - \dot{\varepsilon}_1^2)\rho^3}\\ &+ \begin{pmatrix}-\psi(t) - \frac{3x^2}{\rho^2}\\ \frac{-3xy}{\rho^2}\end{pmatrix}\frac{\dot{\varepsilon}_1^2\dot{\varepsilon}_2^2\,\Lambda\,[u(t_{\mathrm{v}1}) - u(t_{\mathrm{v}2})]}{2\pi(\dot{\varepsilon}_2^2 - \dot{\varepsilon}_1^2)\rho^3[\Lambda\,\psi(t)]^{5/2}}\end{aligned} \tag{23}$$

where

$$\Lambda = \Gamma Q = \varepsilon_{\rm v1}\varepsilon_{\rm v2}\frac{\varepsilon_{\rm h2}-\varepsilon_{\rm h1}}{\varepsilon_{\rm v2}-\varepsilon_{\rm v1}}$$
$$\psi(t) = \frac{\Psi(t)}{Q\rho^2} = \frac{t^2}{Q\rho^2} - 1.$$

Interchanging x and y in the expression of $E_{x//x//}$ (or $E_{y//x//}$) gives the field $E_{y//y//}$ (or $E_{x//y//}$). Note that the vertical permittivities $\varepsilon_{\rm v1}$ and $\varepsilon_{\rm v2}$ do not affect the coefficients of the δ functions but only the retardations $c_{\rm v1}^{-1}\rho$ and $c_{\rm v2}^{-1}\rho$. From (23), the longitudinal (radial) and transverse (azimuthal) fields are calculated as

$$\begin{aligned}\begin{pmatrix} E_{\rho//x//} \\ E_{\phi//x//}\end{pmatrix} &= \begin{pmatrix} 0 \\ \frac{y}{\rho}\end{pmatrix}\frac{\varepsilon_{\rm h1}\eta_{\rm h1}\delta(t_{\rm h1}) - \varepsilon_{\rm h2}\eta_{\rm h2}\delta(t_{\rm h2})}{2\pi(\varepsilon_{\rm h2}-\varepsilon_{\rm h1})\rho^2} \\ &+ \begin{pmatrix} \frac{x}{\rho} \\ 0\end{pmatrix}\frac{\eta_{\rm h1}\delta(t_{\rm v1}) + \eta_{\rm h2}\delta(t_{\rm v2})}{2\pi\rho^2} \\ &+ \begin{pmatrix} \frac{x}{\rho} \\ \frac{2y}{\rho}\end{pmatrix}\frac{u(t_{\rm h1}) - u(t_{\rm h2})}{2\pi(\varepsilon_{\rm h2}-\varepsilon_{\rm h1})\rho^3} \\ &+ \begin{pmatrix} \frac{-2x}{\rho} \\ \frac{-y}{\rho}\end{pmatrix}\frac{\dot\varepsilon_1 u(t_{\rm v1}) - \dot\varepsilon_2 u(t_{\rm v2})}{2\pi(\dot\varepsilon_2^2-\dot\varepsilon_1^2)\rho^3} \\ &+ \begin{pmatrix} \frac{-x}{\rho}[\psi(t)+3] \\ \frac{y}{\rho}\psi(t)\end{pmatrix}\frac{\dot\varepsilon_1^2\dot\varepsilon_2^2\Lambda\,[u(t_{\rm v1})-u(t_{\rm v2})]}{2\pi(\dot\varepsilon_2^2-\dot\varepsilon_1^2)\rho^3[\Lambda\,\psi(t)]^{5/2}}.\end{aligned} \tag{24}$$

With $\varepsilon_{\rm h1} = \varepsilon_{\rm v1} < \min\{\varepsilon_{\rm h2}, \varepsilon_{\rm v2}\}$, one can obtain the HH-case formulas in [24], for which the present parameter Γ is positive. Further setting $\varepsilon_{\rm h2} = \varepsilon_{\rm v2}$ gives the formulas for the isotropic case, equal to (or consistent with) those in [4], [16], and [17]. The fourth term on the right-hand side of (23) determines the static fields that remain after $t = \max\{c_{\rm h\bar p}^{-1}\rho, c_{\rm v\bar q}^{-1}\rho\}$

$$\begin{pmatrix} \frac{y^2-2x^2}{\rho^2} \\ \frac{-3xy}{\rho^2}\end{pmatrix}\frac{-1}{2\pi(\dot\varepsilon_1+\dot\varepsilon_2)\rho^3}.$$

Using (23), one can obtain realistic waveforms by the time convolution ($\otimes$) with a smooth source signal $g(t)$. Fig. 3 shows the waveforms of $E_{x//x//} \otimes g(t)$ calculated with the values in Table I, for $g(t) = 10^{-9}\delta_T(t)$ where $\delta_T(t) = (\pi^{1/2}T)^{-1}e^{-t^2/T^2}$. One can see the effect of the uniaxiality on the impulse arrivals: the leading impulse near $t = 47.2$ ns in Fig. 3(a) separates into the impulses at $c_{\rm h1}^{-1}\rho \approx 47.2$ (or 57.8 ns) and $c_{\rm v1}^{-1}\rho \approx 57.8$ (or 47.2 ns) in Fig. 3(b) [or Fig. 3(c)], and the lagging impulse near 124.8 ns separates into the impulses at $c_{\rm h2}^{-1}\rho \approx 124.8$ (or 133.4 ns) and $c_{\rm v2}^{-1}\rho \approx 133.4$ (or 124.8 ns). The negative peak in Fig. 3(a) and similar peaks in Fig. 3(b) and (c) are due to the last term of (23).

The coefficients of the δ functions in (23) are proportional to ρ^{-2}, like the coefficients of the "minor tremors" in the classical elastic "three-dimensional problem" of [18]. All the step function terms are (or, can be regarded as) proportional to ρ^{-3} except in some limiting cases. At the interface, there do not appear the singularities in the sharpness of $\delta'(t)[= \partial_t\delta(t)]$ or $\mathcal{H}\delta'(t)$ that suggest the spherical space waves (see Section V; $\mathcal{H}$ is the Hilbert transform). For the HH case, therefore, and for the VV case in Section III-B, the interfacial far fields in the time domain are dominated by the impulse components, provided that the source signal has a sufficiently short duration.

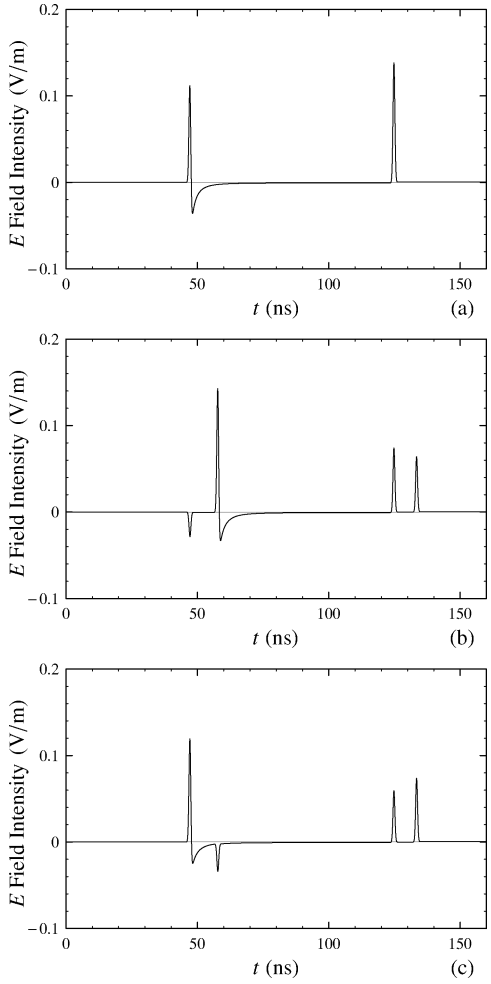

Fig. 3. The HH-case waveforms calculated by $E_{x//x//} \otimes 10^{-9}\,\delta_{(500\ \rm ps)}(t)$ at $(x, y) = (10, 10)$m for (a) $(\varepsilon_{\rm h1}, \varepsilon_{\rm v1}, \varepsilon_{\rm h2}, \varepsilon_{\rm v2}) = (1, 1, 7, 7)\varepsilon_0$, (b) $(\varepsilon_{\rm h1}, \varepsilon_{\rm v1}, \varepsilon_{\rm h2}, \varepsilon_{\rm v2}) = (1, 1.5, 7, 8)\varepsilon_0$, and (c) $(\varepsilon_{\rm h1}, \varepsilon_{\rm v1}, \varepsilon_{\rm h2}, \varepsilon_{\rm v2}) = (1.5, 1, 8, 7)\varepsilon_0$. The positive peaks in (a) are the impulse components that separate into those in (b) and (c) under uniaxiality. The negative peak in (a) and similar (slow-decaying) peaks in (b) and (c) are not impulse components.

B. The VV Case

Explicit solutions are also available for the VV case [Fig. 1(b)]. Because $\mathring{J}_z$ does not appear in (2)–(4), the TE fields are not excited and there occurs no such phenomenon as the wavefront separation into the TE and TM ones. Solving (5)–(7) for $\mathring{J}_z = \delta(z - 0^+)$ (with $\mathring{J}_k = 0$ and $\mathring{J}_\alpha = 0$), the vertical E fields in the physical domain [except at $(x, y) = (0, 0)$] can be written as

$$E_{z'z'} = \mathcal{C}^{\rm i}\left\{-\frac{jk\mathring{H}_{\alpha//z'}}{s\,\varepsilon_{\rm v1}}\right\} = -\frac{\partial_x^2+\partial_y^2}{\varepsilon_{\rm v1}^2}\mathcal{C}^{\rm i}\left\{\frac{s^{-1}}{V_1+V_2}\right\} \tag{25}$$
$$E_{z,z'} = \mathcal{C}^{\rm i}\left\{-\frac{jk\mathring{H}_{\alpha//z'}}{s\,\varepsilon_{\rm v2}}\right\} = \frac{\varepsilon_{\rm v1}}{\varepsilon_{\rm v2}}E_{z'z'} \tag{26}$$

just above and just below the interface, respectively. The marks $'$ and $,$ indicate the superjacency and subjacency, respectively, of

the interfacial antennas. The field $\mathring{H}_{\alpha\prime\prime z'}$ is $jk/[s\,\varepsilon_{\rm v1}(Z_1^{\rm TM}+Z_2^{\rm TM})]$.

The expression $\mathcal{C}^{\rm i}\{s^{-1}/(V_1+V_2)\}$ in (25) can be expanded, similarly as in (18), as

$$\sum_{n=1}^{2}\frac{\dot\varepsilon_n\dot\varepsilon_{\bar n}^2}{\dot\varepsilon_{\bar n}^2-\dot\varepsilon_n^2}\mathcal{C}^{\rm i}\left\{\frac{\frac{\gamma_{vn}}{s}}{k^2+s^2Q}\right\} \tag{27}$$

where the $\mathcal{C}^{\rm i}\{\,\}$ part can be *replaced* with

$$\frac{u(t_{\rm vn})}{2\pi\rho}\,I\!\left(\frac{\Psi(t)}{\check t_{\rm vn}^2}\right)=\frac{u(t_{\rm vn})}{2\pi}\left[\frac{1}{\rho}-\frac{\dot\varepsilon_n\,U(t)}{[\Gamma\Psi(t)]^{1/2}}\right] \tag{28}$$

by the procedure that leads to (20). Carrying out a lengthy calculation for $\partial_x^2+\partial_y^2\,[=\rho^{-1}\partial_\rho(\rho\,\partial_\rho)]$ in (25) with (27) and (28), one can obtain

$$\begin{aligned}E_{z'z'}=&\frac{-\frac{\dot\varepsilon_2^2}{\dot\varepsilon_1}\eta_{\rm v1}}{\varepsilon_{\rm v2}-\varepsilon_{\rm v1}}\frac{\delta(t_{\rm v1})}{2\pi\rho^2}+\frac{\varepsilon_{\rm v2}^2}{\varepsilon_{\rm v1}^2}\frac{\frac{\dot\varepsilon_1^2}{\dot\varepsilon_2}\eta_{\rm v2}}{\varepsilon_{\rm v2}-\varepsilon_{\rm v1}}\frac{\delta(t_{\rm v2})}{2\pi\rho^2}\\&+\frac{-\dot\varepsilon_1^2\,\dot\varepsilon_2^2}{\varepsilon_{\rm v1}^2(\dot\varepsilon_2^2-\dot\varepsilon_1^2)}\left[\frac{1}{\dot\varepsilon_1}\frac{u(t_{\rm v1})}{2\pi\rho^3}-\frac{1}{\dot\varepsilon_2}\frac{u(t_{\rm v2})}{2\pi\rho^3}\right]\\&+[2\,\psi(t)+3]\frac{\dot\varepsilon_1^2\,\dot\varepsilon_2^2\,\Lambda^2\,[u(t_{\rm v1})-u(t_{\rm v2})]}{2\pi\varepsilon_{\rm v1}^2(\dot\varepsilon_2^2-\dot\varepsilon_1^2)\rho^3[\Lambda\,\psi(t)]^{5/2}}\end{aligned} \tag{29}$$

where $\eta_{\rm vn}=(\mu/\varepsilon_{\rm vn})^{1/2}$. The third term on the right determines the static field that remains after $t=c_{\rm v\bar q}^{-1}\rho$

$$\frac{-\dot\varepsilon_1\dot\varepsilon_2}{2\pi\varepsilon_{\rm v1}^2(\dot\varepsilon_1+\dot\varepsilon_2)\rho^3}.$$

The field just below the interface $E_{z\prime z'}$ is obtained using (26). Setting $\varepsilon_{\rm h1}=\varepsilon_{\rm v1}$ and $\varepsilon_{\rm h2}=\varepsilon_{\rm v2}$ gives the isotropic VV-case formulas in [15] and [16]. A waveform is shown in Fig. 4, obtained by the convolution $E_{z'z'}\otimes 10^{-9}\delta_T(t)$ for the values in the last column of Table I. The conspicuous peaks near $t=33.4$ ns and 57.8 ns are due to the $\delta(t_{\rm v1})$ and $\delta(t_{\rm v2})$ terms, respectively. The decaying small peak just after 33.4 ns is due to the last term of (29).

C. The HV Case

In the HV case [Fig. 1(c)], the E fields are of the TM type

$$E_{z'x\prime\prime}=\mathcal{C}_{\rm c}^{\rm i}\left\{-\frac{jk\mathring{H}_{\alpha'k\prime\prime}}{s\,\varepsilon_{\rm v1}}\right\}=\frac{-1}{\varepsilon_{\rm v1}}\mathcal{L}^{\rm i}\left\{\frac{\partial_x}{s}\mathcal{B}^{\rm i}\left\{\frac{V_2}{V_1+V_2}\right\}\right\} \tag{30}$$

$$E_{z\prime x\prime\prime}=\mathcal{C}_{\rm c}^{\rm i}\left\{-\frac{jk\mathring{H}_{\alpha\prime k\prime\prime}}{s\,\varepsilon_{\rm v2}}\right\}=\frac{\varepsilon_{\rm v1}}{\varepsilon_{\rm v2}}E_{z'x\prime\prime}\left(+\frac{\partial_x\delta(\boldsymbol{\rho})u(t)}{\varepsilon_{\rm v2}}\right) \tag{31}$$

which can be obtained from (5)–(7) with (1). Here

$$(\mathring{H}_{\alpha'k\prime\prime},\mathring{H}_{\alpha\prime k\prime\prime})=\frac{(-Z_2^{\rm TM},Z_1^{\rm TM})}{Z_1^{\rm TM}+Z_2^{\rm TM}}$$

and $\mathcal{C}_{\rm c}^{\rm i}\{\,\}=\mathcal{C}^{\rm i}\{(\,)\cos\alpha\}$.

Consider $E_{z'x\prime\prime}$ in (30). The k integral implied in the $\mathcal{B}^{\rm i}\{\,\}$ part does not converge. The asymptotic quantity $\dot\varepsilon_1/(\dot\varepsilon_1+\dot\varepsilon_2)$ has to be subtracted from the operand $V_2/(V_1+V_2)$. This subtraction does not affect the field at $(x,y)\neq(0,0)$, but is a step

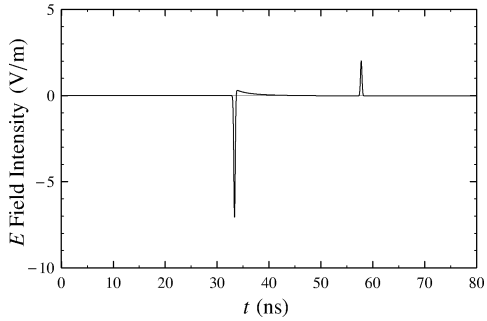

Fig. 4. The VV-case waveform calculated by $E_{z'z'}\otimes 10^{-9}\delta_{(200\ \rm ps)}(t)$ at $(x,y)=(10,0)$ m for $(\varepsilon_{\rm h1},\varepsilon_{\rm v1},\varepsilon_{\rm h2},\varepsilon_{\rm v2})=(1.5,1,3.5,3)\varepsilon_0$. The conspicuous peaks near $t=33.4$ and 57.8 ns are the impulse components, while the decaying small peak just after 33.4 ns is not.

TABLE I
NUMERICAL VALUES FOR COMPUTATION OF THE E FIELD WAVEFORMS[a]

	Fig. 3(a)	Figs. 3(b) and 7	Fig. 3(c)	Figs. 4, 5, 8, and 9
$\varepsilon_{\rm h1}$	ε_0	ε_0	$1.5\varepsilon_0$	$1.5\varepsilon_0$
$\varepsilon_{\rm v1}$	ε_0	$1.5\varepsilon_0$	ε_0	ε_0
$\varepsilon_{\rm h2}$	$7\varepsilon_0$	$7\varepsilon_0$	$8\varepsilon_0$	$3.5\varepsilon_0$
$\varepsilon_{\rm v2}$	$7\varepsilon_0$	$8\varepsilon_0$	$7\varepsilon_0$	$3\varepsilon_0$
(x,y), m	$(10,10)$	$(10,10)$	$(10,10)$	$(10,0)$
T, ps	500	500	500	200

[a]Here ε_0 is the free-space permittivity.

for mathematical strictness [16]. Then the $s^{-1}\partial_x\mathcal{B}^{\rm i}\{\,\}$ part in (30) can be written as

$$\frac{-s^2}{\pi^2}\frac{\dot\varepsilon_1\dot\varepsilon_2}{\dot\varepsilon_2^2-\dot\varepsilon_1^2}\frac{x}{\rho^3}\int_{c_{\rm v\bar q}^{-1}\rho}^{c_{\rm vq}^{-1}\rho}\frac{\check\tau_{\rm vq}\hat\tau_{\rm v\bar q}}{\rho\,\Psi(\tau)}\tau^2K_1(s\tau)\,{\rm d}\tau \tag{32}$$

where $\check\tau_{\rm vq}=(\tau^2-c_{\rm vq}^{-2}\rho^2)^{1/2}$ and $\hat\tau_{\rm v\bar q}=(c_{\rm v\bar q}^{-2}\rho^2-\tau^2)^{1/2}$. Use has been made of (i) $\partial_xH_0^{(2)}(k\rho)=-(x/\rho)kH_1^{(2)}(k\rho)$; (ii) the variable change $k=-js\tau/\rho$; and (iii) $H_1^{(2)}(-js\tau)=-(2/\pi)K_1(s\tau)$ [22, p. 375]. By $\mathcal{L}^{\rm i}\{K_1(s\tau)\}=(t/\tau)u(t-\tau)/(t^2-\tau^2)^{1/2}$ [25, p. 363], the field $E_{z'x\prime\prime}$ becomes

$$E_{z'x\prime\prime}=\frac{1}{2\pi\varepsilon_{\rm v1}}\frac{\dot\varepsilon_1\dot\varepsilon_2}{\dot\varepsilon_2^2-\dot\varepsilon_1^2}\frac{x}{\rho^3}\partial_t^2(tA) \tag{33}$$

where

$$\begin{aligned}A=&\frac{2}{\pi}\int_{c_{\rm v\bar q}^{-1}\rho}^{c_{\rm vq}^{-1}\rho}\frac{\tau\,\check\tau_{\rm vq}\hat\tau_{\rm v\bar q}\,u(t-\tau)}{\rho\,\Psi(\tau)(t^2-\tau^2)^{1/2}}\,{\rm d}\tau\\=&\check t_{\rm vq}^2\Big\{\grave B\big[u(t_{\rm vq})-u(t_{\rm v\bar q})\big]+\acute B\,u(t_{\rm v\bar q})\Big\}\end{aligned} \tag{34}$$

with the B factors given by

$$(\grave B,\acute B)=\frac{2}{\pi}\int_{(0,\kappa)}^{\pi/2}\frac{\big[(\hat t_{\rm v\bar q}^2,-\check t_{\rm v\bar q}^2)+\check t_{\rm vq}^2\sin^2\beta\big]^{1/2}}{\rho\,[\Psi(t)-\check t_{\rm vq}^2\sin^2\beta]}\cos^2\beta\,{\rm d}\beta. \tag{35}$$

$(\kappa=\sin^{-1}(\check t_{\rm v\bar q}/\check t_{\rm vq}))$. Here $\hat t_{\rm v\bar q}=(c_{\rm v\bar q}^{-2}\rho^2-t^2)^{1/2}$ and $\check t_{\rm v(q,\bar q)}=(t^2-c_{\rm v(q,\bar q)}^{-2}\rho^2)^{1/2}$. The integrands for $\grave B$ and $\acute B$

are practically the same. The relation between τ and β is $(t^2-\tau^2)^{1/2}=\check{t}_{\mathrm{v}\mathfrak{q}}\sin\beta$.

The expressions for $\grave{B}$ and $\acute{B}$ cannot be obtained in integral-free forms, though one may write them in terms of the elliptic integrals with extended range of modulus k ($-\infty<k<1$)

$$E_{\pm}(\varphi,k)=\int_0^{\varphi}(1-k\sin^2\beta)^{\pm 1/2}\,\mathrm{d}\beta \tag{36}$$

$$\Pi(\varphi,n,k)=\int_0^{\varphi}\frac{(1-k\sin^2\beta)^{-1/2}}{1-n\sin^2\beta}\,\mathrm{d}\beta. \tag{37}$$

For example, $\grave{B}$ in (35) can be expressed as

$$\grave{B}=\frac{\hat{t}_{\mathrm{v}\bar{\mathfrak{q}}}}{\rho\,\Psi(t)}\left[\frac{(n-1)k}{n^2}\frac{E_-\left(\frac{\pi}{2},k\right)}{\frac{\pi}{2}}+\frac{1}{n}\frac{E_+\left(\frac{\pi}{2},k\right)}{\frac{\pi}{2}}+\frac{(n-1)(n-k)}{n^2}\frac{\Pi\left(\frac{\pi}{2},n,k\right)}{\frac{\pi}{2}}\right] \tag{38}$$

where $k=-\check{t}^2_{\mathrm{v}\mathfrak{q}}/\hat{t}^2_{\mathrm{v}\bar{\mathfrak{q}}}$ and $n=\check{t}^2_{\mathrm{v}\mathfrak{q}}/\Psi(t)$. The use of the elliptic integrals is also found in seismological studies [19], [26, Sec. 7.6.4].

Unfortunately, the elliptic integrals do not give an immediate insight into the wave physics. It is not a fruitful work to express the t derivatives of the elliptic integrals [related with ∂_t^2 in (33)] in terms of ∂_t-free expressions, even if it might be possible. It is preferred to assume a smooth source signal $g(t)$ and calculate the waveform numerically by the convolution

$$E_{z'x''}\otimes g(t)=\frac{1}{2\pi\varepsilon_{\mathrm{v}1}}\frac{\dot{\varepsilon}_1\dot{\varepsilon}_2}{\dot{\varepsilon}_2^2-\dot{\varepsilon}_1^2}\frac{x}{\rho^3}\left[\partial_t^2 g(t)\right]\otimes(tA) \tag{39}$$

where A is evaluated using (35). Equation (39) involves a double integration: one integral for the convolution ($\otimes$) and the other contained in the expression of A. Fig. 5(a) shows a waveform of (39) with $g(t)=10^{-9}\delta_T(t)$, calculated for the values in Table I.

Although an integral-free expression for $E_{z'x''}$ is not available, the leading impulse component (at $c_{\mathrm{v}\mathfrak{q}}^{-1}\rho$) can be extracted as follows. Consider (33), in which tA is equal to $\check{t}^2_{\mathrm{v}\mathfrak{q}}\,t\,\grave{B}$ for $c_{\mathrm{v}\mathfrak{q}}^{-1}\rho<t<c_{\mathrm{v}\bar{\mathfrak{q}}}^{-1}\rho$. Because $\grave{B}$ and $\partial_t\grave{B}$ have finite values at $t=c_{\mathrm{v}\mathfrak{q}}^{-1}\rho$, the first-order derivative $\partial_t(tA)$ has no singularity at $c_{\mathrm{v}\mathfrak{q}}^{-1}\rho$ but at most a finite jump (from zero) of amount

$$\lim_{t\to(c_{\mathrm{v}\mathfrak{q}}^{-1}\rho)^+}\partial_t(tA)=\lim_{t\to c_{\mathrm{v}\mathfrak{q}}^{-1}\rho}\left[2t^2\grave{B}+\check{t}^2_{\mathrm{v}\mathfrak{q}}\partial_t(t\grave{B})\right]=\left(\frac{\mu}{\varepsilon_{\mathrm{v}\mathfrak{q}}}\right)^{1/2}\frac{\frac{\varepsilon_{\mathrm{v}\mathfrak{q}}}{\dot{\varepsilon}_{\mathfrak{q}}}(\dot{\varepsilon}^2_{\bar{\mathfrak{q}}}-\dot{\varepsilon}^2_{\mathfrak{q}})}{[\varepsilon_{\mathrm{h}\mathfrak{q}}(\varepsilon_{\mathrm{v}\bar{\mathfrak{q}}}-\varepsilon_{\mathrm{v}\mathfrak{q}})]^{1/2}} \tag{40}$$

which is none other than the coefficient of $\delta(t_{\mathrm{v}\mathfrak{q}})$ in the waveform of $\partial_t^2(tA)$. Then $E_{z'x''}$ in (33) can be written as

$$E_{z'x''}=\eta_{\mathrm{v}\mathfrak{q}}\frac{\varepsilon_{\mathrm{v}\mathfrak{q}}}{\varepsilon_{\mathrm{v}1}}\frac{\dot{\varepsilon}_{\bar{\mathfrak{q}}}\,\mathrm{sgn}(\varepsilon_{\mathrm{v}2}-\varepsilon_{\mathrm{v}1})}{[\varepsilon_{\mathrm{h}\mathfrak{q}}(\varepsilon_{\mathrm{v}\bar{\mathfrak{q}}}-\varepsilon_{\mathrm{v}\mathfrak{q}})]^{1/2}}\frac{x}{\rho}\frac{\delta(t_{\mathrm{v}\mathfrak{q}})}{2\pi\rho^2}+\cdots. \tag{41}$$

Note that the extracted impulse component is proportional to ρ^{-2}. This component is important in connection with the lateral head wave; see Section IV. Fig. 5(b) compares the waveform of the impulse component (dotted line) against the numerical waveform in Fig. 5(a) (solid line).

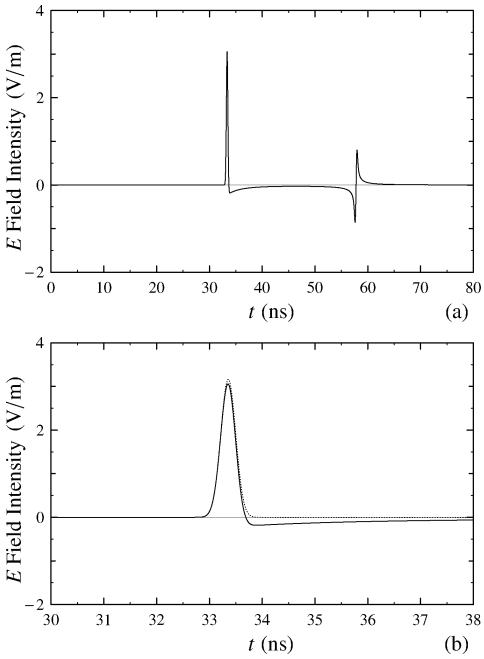

Fig. 5. The waveforms of the HV case. (a) Waveform of $E_{z'x''}\otimes 10^{-9}\delta_{(200\ \mathrm{ps})}(t)$ obtained from (39) at $(x,y)=(10,0)\,\mathrm{m}$ for $(\varepsilon_{\mathrm{h}1},\varepsilon_{\mathrm{v}1},\varepsilon_{\mathrm{h}2},\varepsilon_{\mathrm{v}2})=(1.5,1,3.5,3)\varepsilon_0$. (b) Waveform of the analytically extracted impulse component (dotted line) compared with the numerical waveform in (a) (solid line).

Now consider the waveform near $t=c_{\mathrm{v}\bar{\mathfrak{q}}}^{-1}\rho$. It turns out that

$$\partial_t(tA)=\partial_t\left(\check{t}^2_{\mathrm{v}\mathfrak{q}}\,t\,\grave{B}\right)\to-\infty\ \ (\text{for } t\to(c_{\mathrm{v}\bar{\mathfrak{q}}}^{-1}\rho)^-) \tag{42a}$$

$$=\partial_t\left(\check{t}^2_{\mathrm{v}\mathfrak{q}}\,t\,\acute{B}\right)\to-\infty\ \ (\text{for } t\to(c_{\mathrm{v}\bar{\mathfrak{q}}}^{-1}\rho)^+). \tag{42b}$$

Upon a careful examination, one can find out that the main trends of divergence in (42a) and (42b) are the same. Hence $E_{z'x''}$ [which has the second-derivative factor $\partial_t^2(tA)$] does not possess an impulse component at $t=c_{\mathrm{v}\bar{\mathfrak{q}}}^{-1}\rho$. Instead, $E_{z'x''}$ diverges negatively for $t\to(c_{\mathrm{v}\bar{\mathfrak{q}}}^{-1}\rho)^-$ and positively for $t\to(c_{\mathrm{v}\bar{\mathfrak{q}}}^{-1}\rho)^+$; see the waveform near $t=57.8$ ns in Fig. 5(a). It can be shown that this singularity is of the type $(-\pi t_{\mathrm{v}\bar{\mathfrak{q}}})^{-1}$, which overwhelms another singularity of the type $\ln|t_{\mathrm{v}\bar{\mathfrak{q}}}|$. Derivation of these singularities is not presented due to space limitations.

Interchanging x and y in the expressions of $E_{z'x''}$ and $E_{z'x''}$ gives the fields of the y-directional source, $E_{z'y''}$ and $E_{z'y''}$.

D. The VH Case

In the VH case [Fig. 1(d)], the E field is horizontal and is continuous at the interface except at $(x,y)=(0,0)$. Solving (5) and (6), the E field components are written as

$$\begin{pmatrix}E_{x''z'}\\E_{y''z'}\end{pmatrix}=\begin{pmatrix}\mathcal{C}_{\mathrm{c}}^{\mathrm{i}}\\\mathcal{C}_{\mathrm{s}}^{\mathrm{i}}\end{pmatrix}\{-Z_2^{\mathrm{TM}}\mathring{H}_{\alpha''z'}\}=\frac{1}{\varepsilon_{\mathrm{v}1}}\mathcal{L}^{\mathrm{i}}\left\{\frac{1}{s}\begin{pmatrix}\partial_x\\\partial_y\end{pmatrix}\mathcal{B}^{\mathrm{i}}\left\{\frac{V_2}{V_1+V_2}\right\}\right\} \tag{43}$$

with $\mathring{H}_{\alpha//z'}$ in Section III-B; here $\mathcal{C}_{\rm s}^{\rm i}\{\,\} = \mathcal{C}^{\rm i}\{(\,)\sin\alpha\}$. Comparing these E fields with those of the HV case, it can be noticed that $E_{x//z'} = -E_{z'x//}$ and $E_{y//z'} = -E_{z'y//}$. The impulse components extractable from (43) are

$$-\eta_{\rm vq}\frac{\varepsilon_{\rm vq}}{\varepsilon_{\rm v1}}\frac{\dot{\varepsilon}_{\bar{\rm q}}\,{\rm sgn}(\varepsilon_{\rm v2}-\varepsilon_{\rm v1})}{[\varepsilon_{\rm hq}(\varepsilon_{\rm v\bar{q}}-\varepsilon_{\rm vq})]^{1/2}}\begin{pmatrix}\frac{x}{\rho}\\ \frac{y}{\rho}\end{pmatrix}\frac{\delta(t_{\rm vq})}{2\pi\rho^2}$$

from which the radial field is obtained as

$$E_{\rho//z'} = -\eta_{\rm vq}\frac{\varepsilon_{\rm vq}}{\varepsilon_{\rm v1}}\frac{\dot{\varepsilon}_{\bar{\rm q}}\,{\rm sgn}(\varepsilon_{\rm v2}-\varepsilon_{\rm v1})}{[\varepsilon_{\rm hq}(\varepsilon_{\rm v\bar{q}}-\varepsilon_{\rm vq})]^{1/2}}\frac{\delta(t_{\rm vq})}{2\pi\rho^2}+\cdots. \quad (44)$$

The azimuthal field $E_{\phi//z'}$ is identically zero, as can be inferred from (43).

E. The H Fields

For the horizontal source $\mathbf{J} = \mathbf{i}_x\delta(\boldsymbol{\rho})\delta(z)\delta(t)$, the horizontal H fields in the FL domain are obtained from (2), (3), (5), and (6) [with (1)] as

$$\begin{pmatrix}\mathring{H}_{x'x//} & \mathring{H}_{y'x//}\\ \mathring{H}_{x\prime x//} & \mathring{H}_{y\prime x//}\end{pmatrix} = \begin{pmatrix}\frac{1}{Z_1^{\rm TE}}\\ -\frac{1}{Z_2^{\rm TE}}\end{pmatrix}\begin{pmatrix}-\mathring{E}^{\rm TE}_{y//x//} & \mathring{E}^{\rm TE}_{x//x//}\end{pmatrix} + \begin{pmatrix}\frac{1}{Z_1^{\rm TM}}\\ -\frac{1}{Z_2^{\rm TM}}\end{pmatrix}\begin{pmatrix}-\mathring{E}^{\rm TM}_{y//x//} & \mathring{E}^{\rm TM}_{x//x//}\end{pmatrix} \quad (45)$$

where the $\mathring{E}$ fields are given in (10) and (11). The relation $\mathring{H}_{x'x//} - \mathring{H}_{x\prime x//} = 0$ implies the interfacial continuity of the space-domain field. The relation $\mathring{H}_{y'x//} - \mathring{H}_{y\prime x//} = -1$ also implies the continuity, since $\mathcal{C}^{\rm i}\{\mathring{H}_{y'x//} - \mathring{H}_{y\prime x//}\} = -\delta(\boldsymbol{\rho})\delta(t)$. The physical domain fields are not integral-free; they are written (similarly as $E_{z'x//}$ in Section III-C) as

$$\begin{aligned}&\begin{pmatrix}H_{x//x//}\\ H_{y//x//}\end{pmatrix}\\ &= \frac{1}{\mu(\varepsilon_{\rm h2}-\varepsilon_{\rm h1})}\left[\begin{pmatrix}\frac{xy}{\rho^2}\\ \frac{y^2}{\rho^2}\end{pmatrix}\frac{\rho\,\partial_t^2 A_0^{\rm TE}}{2\pi\rho^2} + \begin{pmatrix}\frac{2xy}{\rho^2}\\ \frac{y^2-x^2}{\rho^2}\end{pmatrix}\frac{\partial_t(tA_1^{\rm TE})}{2\pi\rho^3}\right]\\ &\quad + \frac{\dot{\varepsilon}_1\dot{\varepsilon}_2}{Q}\left[\begin{pmatrix}\frac{xy}{\rho^2}\\ \frac{-x^2}{\rho^2}\end{pmatrix}\frac{\rho\,\partial_t^2 A_0^{\rm TM}}{2\pi\rho^2} + \begin{pmatrix}\frac{2xy}{\rho^2}\\ \frac{y^2-x^2}{\rho^2}\end{pmatrix}\frac{\partial_t(tA_1^{\rm TM})}{2\pi\rho^3}\right]\end{aligned} \quad (46)$$

where $A_0^{\rm TM}$ being equal to QA [with A in (34)]

$$\begin{pmatrix}A_0^{\rm TE}\\ A_1^{\rm TE}\end{pmatrix} = \frac{2}{\pi}\int_{c_{\rm h\bar{p}}^{-1}\rho}^{c_{\rm h\bar{p}}^{-1}\rho}\begin{pmatrix}\frac{\tau}{\rho}\\ \frac{\rho}{\tau}\end{pmatrix}\frac{\check{\tau}_{\rm hp}\hat{\tau}_{\rm h\bar{p}}\,u(t-\tau)}{\rho^2(t^2-\tau^2)^{1/2}}\,{\rm d}\tau \quad (47)$$

$$\begin{pmatrix}A_0^{\rm TM}\\ A_1^{\rm TM}\end{pmatrix} = \frac{2}{\pi}\int_{c_{\rm v\bar{q}}^{-1}\rho}^{c_{\rm v\bar{q}}^{-1}\rho}\begin{pmatrix}\frac{\tau}{\rho}\\ \frac{\rho}{\tau}\end{pmatrix}\frac{\check{\tau}_{\rm vq}\hat{\tau}_{\rm v\bar{q}}\,u(t-\tau)}{\rho^2(t^2-\tau^2)^{1/2}\psi(\tau)}\,{\rm d}\tau. \quad (48)$$

After extracting the impulse components, one can write the H fields in the radial and azimuthal directions (in simpler forms than the x- and y-directional fields) as

$$H_{\rho//x//} = \frac{{\rm sgn}(\varepsilon_{\rm h2}-\varepsilon_{\rm h1})}{\left[\frac{(\varepsilon_{\rm h\bar{p}}-\varepsilon_{\rm hp})}{\varepsilon_{\rm hp}}\right]^{1/2}}\frac{y}{\rho}\frac{\delta(t_{\rm hp})}{2\pi\rho^2}+\cdots \quad (49)$$

$$H_{\phi//x//} = -\frac{\dot{\varepsilon}_{\bar{\rm q}}\,{\rm sgn}(\varepsilon_{\rm v2}-\varepsilon_{\rm v1})}{[\varepsilon_{\rm hq}(\varepsilon_{\rm v\bar{q}}-\varepsilon_{\rm vq})]^{1/2}}\frac{x}{\rho}\frac{\delta(t_{\rm vq})}{2\pi\rho^2}+\cdots. \quad (50)$$

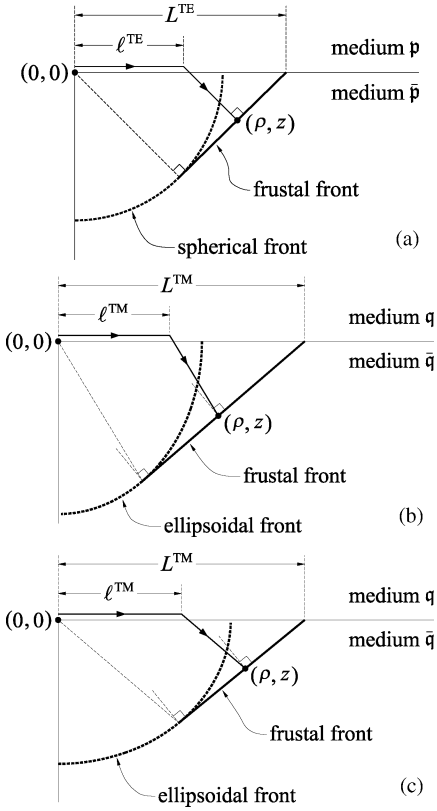

Fig. 6. The frustal fronts and the ray paths of: (a) the TE head wave; (b) the TM head wave for $\varepsilon_{\rm h\bar{q}} < \varepsilon_{\rm v\bar{q}}$ (i.e., $\chi_{\bar{\rm q}} < 1$); and (c) the TM head wave for $\varepsilon_{\rm h\bar{q}} > \varepsilon_{\rm v\bar{q}}$ (i.e., $\chi_{\bar{\rm q}} > 1$). The TM rays are not normal to the frustal fronts.

The impulse components in (49) and (50) are related with the TE and TM waves, respectively.

The vertical field of the horizontal source is calculated [similarly as (12) through (17)] as

$$\begin{aligned}H_{z//x//} &= \mathcal{C}_{\rm s}^{\rm i}\left\{-\frac{jk}{s\mu}\mathring{E}_{\alpha//\alpha//}\right\}\\ &= \frac{y}{\rho}\left[\frac{\varepsilon_{\rm h1}\delta(t_{\rm h1})-\varepsilon_{\rm h2}\delta(t_{\rm h2})}{2\pi(\varepsilon_{\rm h2}-\varepsilon_{\rm h1})\rho^2} + \frac{3t}{\rho}\frac{u(t_{\rm h1})-u(t_{\rm h2})}{2\pi\mu(\varepsilon_{\rm h2}-\varepsilon_{\rm h1})\rho^3}\right].\end{aligned} \quad (51)$$

For the vertical source $\mathbf{J} = \mathbf{i}_z\delta(\boldsymbol{\rho})\delta(z-0^+)\delta(t)$, the horizontal H fields can be written as

$$\begin{pmatrix}H_{x//z'}\\ H_{y//z'}\end{pmatrix} = \begin{pmatrix}-\mathcal{C}_{\rm s}^{\rm i}\\ \mathcal{C}_{\rm c}^{\rm i}\end{pmatrix}\{\mathring{H}_{\alpha//z'}\} = \frac{1}{\varepsilon_{\rm v1}}\begin{pmatrix}\partial_y\\ -\partial_x\end{pmatrix}\mathcal{C}^{\rm i}\left\{\frac{1}{V_1+V_2}\right\} \quad (52)$$

from (5) and (6) [with (1)]. The expression for the $\mathcal{C}^{\rm i}\{\,\}$ part is obtained by differentiating (27) with respect to t. Completing the differentiations ∂_x and ∂_y in (52), one can write the transverse field as

$$H_{\phi//z'} = \frac{\frac{\dot{\varepsilon}_1^2\dot{\varepsilon}_2^2}{\varepsilon_{\rm v1}}}{\varepsilon_{\rm v2}-\varepsilon_{\rm v1}}\left[\frac{\varepsilon_{\rm v1}}{\dot{\varepsilon}_1^3}\frac{\delta(t_{\rm v1})}{2\pi\rho^2} - \frac{\varepsilon_{\rm v2}}{\dot{\varepsilon}_2^3}\frac{\delta(t_{\rm v2})}{2\pi\rho^2} - \frac{3t}{\rho}\frac{\Lambda\,[u(t_{\rm v1})-u(t_{\rm v2})]}{2\pi\mu\,\rho^3[\Lambda\,\psi(t)]^{5/2}}\right] \quad (53)$$

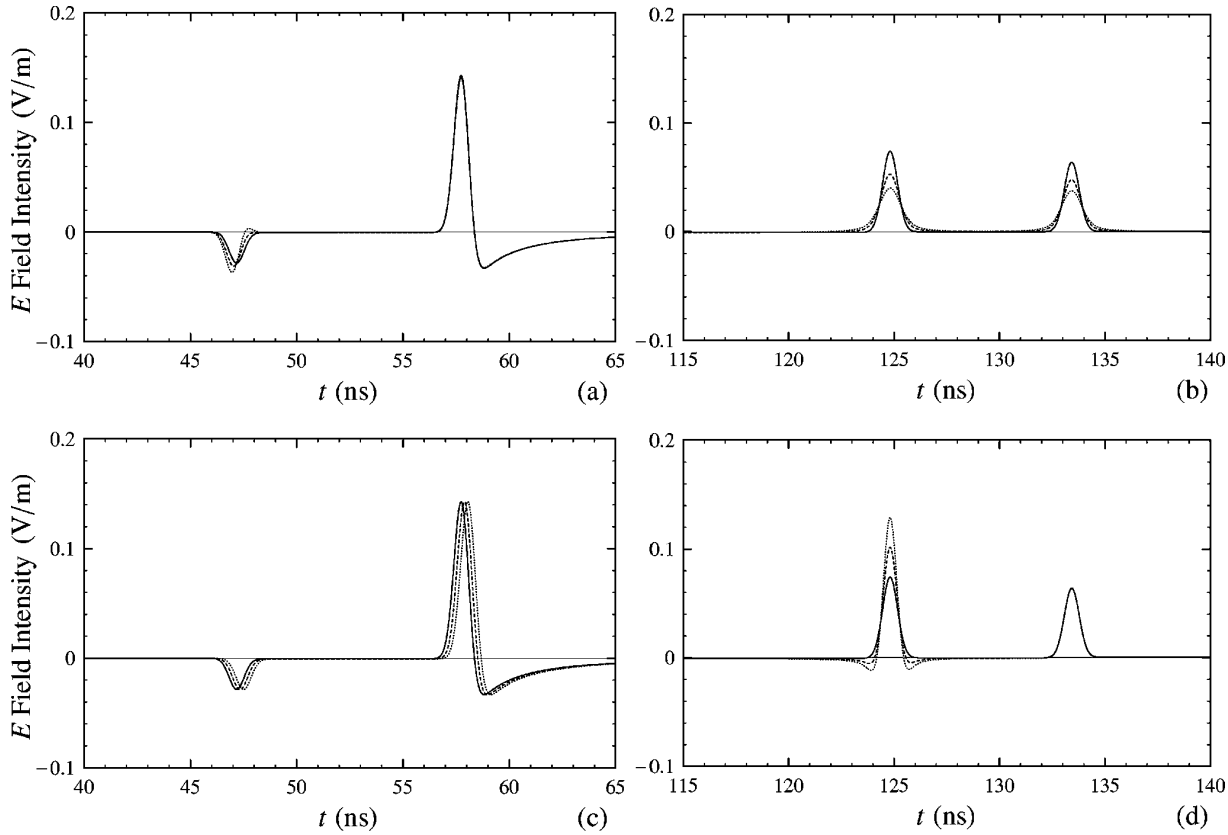

Fig. 7. The effects of the receiver's offset (from the interface) on the HH-case waveform of Fig. 3(b). (a) and (b) Solid, dashed, and dotted curves are for $z = 0$, 2, and 4 cm, respectively. (c) and (d) Solid, dashed, and dotted curves are for $z = 0, -2$, and -4 cm, respectively.

which is consistent with the field in [15]. The radial field $H_{\rho//z'}$ is identically zero.

The vertical field of the vertical source, $H_{z//z'}$, is identically zero, since $\mathring{J}_z$ does not appear in (2)–(4).

IV. Lateral Head Waves

The TE (TM) leading impulse components derived in the previous section [exactly at the interface or infinitesimally within the medium $\bar{\mathfrak{p}}$ (medium $\bar{\mathfrak{q}}$)] pertain to the TE (TM) lateral head wave. A TE head-wave field can be obtained from the leading impulse term of the TE interface solution, by replacing $\rho^{-2}\delta(t_{\mathrm{h}\mathfrak{p}})$ with

$$\frac{\delta\big(t_{\mathrm{h}\mathfrak{p}} - (c_{\mathrm{h}\bar{\mathfrak{p}}}^{-2} - c_{\mathrm{h}\mathfrak{p}}^{-2})^{1/2}|z|\big)}{\rho^{1/2}\Big[\rho - \Big(\frac{\varepsilon_{\mathrm{h}\mathfrak{p}}}{\varepsilon_{\mathrm{h}\bar{\mathfrak{p}}} - \varepsilon_{\mathrm{h}\mathfrak{p}}}\Big)^{1/2}|z|\Big]^{3/2}} = \frac{\delta(t - c_{\mathrm{h}\mathfrak{p}}^{-1}L^{\mathrm{TE}})}{\rho^{1/2}(\ell^{\mathrm{TE}})^{3/2}} \tag{54}$$

for $|z| < [(\varepsilon_{\mathrm{h}\bar{\mathfrak{p}}}/\varepsilon_{\mathrm{h}\mathfrak{p}}) - 1]^{1/2}\rho$ in the medium $\bar{\mathfrak{p}}$. Similarly, a TM head-wave field can be obtained from the leading impulse term of the TM interface solution, by replacing $\rho^{-2}\delta(t_{\mathrm{v}\mathfrak{q}})$ with

$$\frac{\delta\big(t_{\mathrm{v}\mathfrak{q}} - (c_{\mathrm{v}\bar{\mathfrak{q}}}^{-2} - c_{\mathrm{v}\mathfrak{q}}^{-2})^{1/2}\chi_{\bar{\mathfrak{q}}}\,|z|\big)}{\rho^{1/2}\Big[\rho - \Big(\frac{\varepsilon_{\mathrm{v}\mathfrak{q}}}{\varepsilon_{\mathrm{v}\bar{\mathfrak{q}}} - \varepsilon_{\mathrm{v}\mathfrak{q}}}\Big)^{1/2}\chi_{\bar{\mathfrak{q}}}\,|z|\Big]^{3/2}} = \frac{\delta(t - c_{\mathrm{v}\mathfrak{q}}^{-1}L^{\mathrm{TM}})}{\rho^{1/2}(\ell^{\mathrm{TM}})^{3/2}} \tag{55}$$

for $|z| < \chi_{\bar{\mathfrak{q}}}^{-1}[(\varepsilon_{\mathrm{v}\bar{\mathfrak{q}}}/\varepsilon_{\mathrm{v}\mathfrak{q}}) - 1]^{1/2}\rho$ in the medium $\bar{\mathfrak{q}}$. The distances ℓ^{TE}, L^{TE}, ℓ^{TM}, and L^{TM} are described in Fig. 6, where the frustal fronts and the ray paths of the head waves are shown.

From the expressions of $E_{\phi//x//}$, $H_{\rho//x//}$, and $H_{z//x//}$ [in (24), (49), and (51), respectively], it turns out that the Poynting vector of the TE head wave makes a critical angle

$$\theta_{\mathrm{c}}^{\mathrm{TE}} = 90^\circ + \mathrm{sgn}(\varepsilon_{\mathrm{h}2} - \varepsilon_{\mathrm{h}1})\tan^{-1}\left[\left(\frac{\varepsilon_{\mathrm{h}\bar{\mathfrak{p}}}}{\varepsilon_{\mathrm{h}\mathfrak{p}}} - 1\right)^{1/2}\right] \tag{56}$$

with the $+z$ axis. The Poynting vector of the TM head wave makes a critical angle

$$\theta_{\mathrm{c}}^{\mathrm{TM}} = 90^\circ + \mathrm{sgn}(\varepsilon_{\mathrm{v}2} - \varepsilon_{\mathrm{v}1})\tan^{-1}\frac{\left(\frac{\varepsilon_{\mathrm{v}\bar{\mathfrak{q}}}}{\varepsilon_{\mathrm{v}\mathfrak{q}}} - 1\right)^{1/2}}{\chi_{\bar{\mathfrak{q}}}} \tag{57}$$

as can be inferred from $E_{\rho//x//}$, $E_{z'x//}$, $E_{z,x//}$, and $H_{\phi//x//}$ [in (24), (41), (31), and (50), respectively] or from $E_{\rho//z'}$, $E_{z'z'}$, $E_{z,z'}$, and $H_{\phi//z'}$ [in (44), (29), (26), and (53), respectively]. In the present uniaxial case, the critical angle $\theta_{\mathrm{c}}^{\mathrm{TM}}$ is not equal to the front-normal (wave-normal) angle of the TM head wave

$$\theta_{\mathrm{f}}^{\mathrm{TM}} = 90^\circ + \mathrm{sgn}(\varepsilon_{\mathrm{v}2} - \varepsilon_{\mathrm{v}1})\tan^{-1}\frac{\left(\frac{\varepsilon_{\mathrm{v}\bar{\mathfrak{q}}}}{\varepsilon_{\mathrm{v}\mathfrak{q}}} - 1\right)^{1/2}}{\chi_{\bar{\mathfrak{q}}}^{-1}}. \tag{58}$$

The head-wave components of the TE fields yield the impedance $\eta_{\mathrm{h}\bar{\mathfrak{p}}}$, while those of the TM fields yield

$$\left[1 + \frac{\varepsilon_{\mathrm{v}\mathfrak{q}}}{\varepsilon_{\mathrm{v}\bar{\mathfrak{q}}}}(\chi_{\bar{\mathfrak{q}}}^2 - 1)\right]^{1/2}\eta_{\mathrm{h}\bar{\mathfrak{q}}}.$$

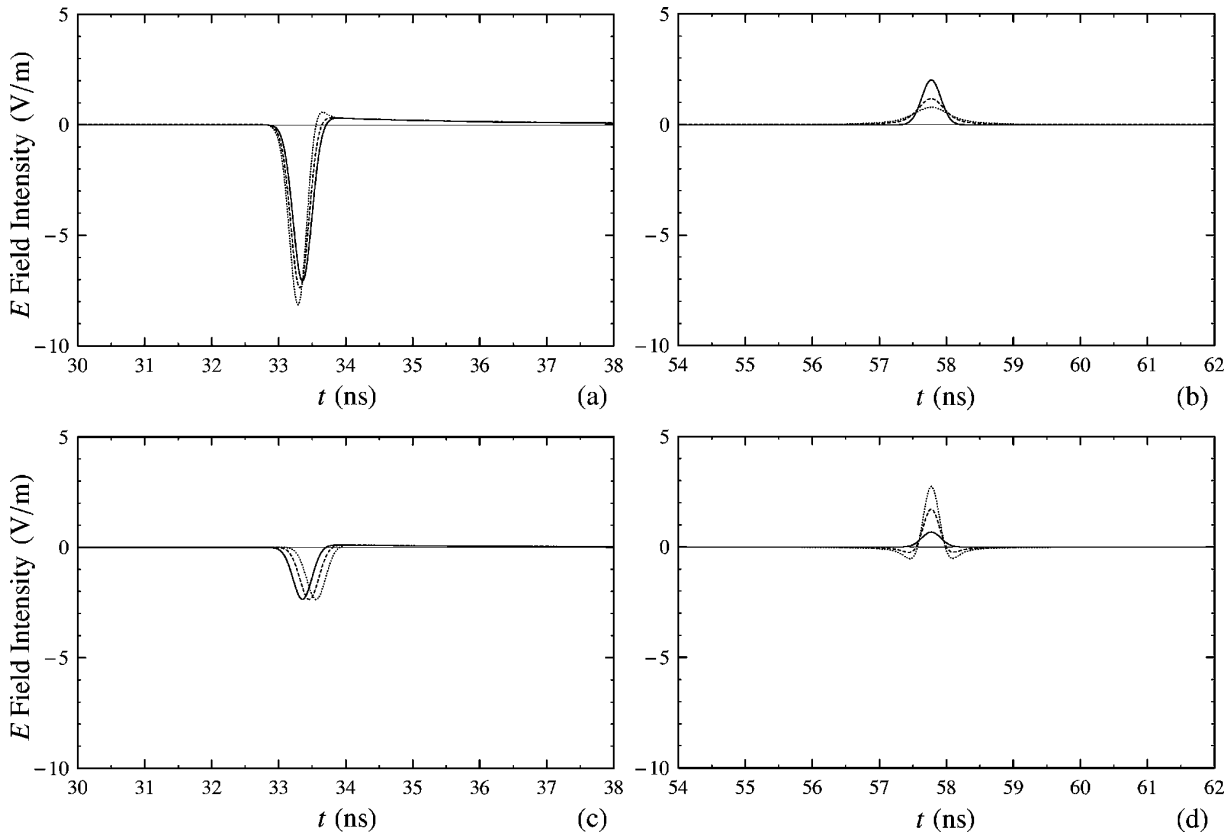

Fig. 8. The effects of the receiver's offset on the VV-case waveform of Fig. 4. (a) and (b) Solid, dashed, and dotted curves are for $z = 0^+$, 2, and 4 cm, respectively. (c) and (d) Solid, dashed, and dotted curves are for $z = 0^-$, -2, and -4 cm, respectively.

V. Effects of Receiver's Small Offset From the Interface

In Section III, the offset of the receiver antenna from the interface is zero or infinitesimally small. Now the receiver is taken a little off the interface by an offset z to see the perturbational effects due to the offset. The waveforms off the interface are computed by the numerical wavenumber–frequency synthesis. The smaller the receiver's offset, the more elaborate synthesis is required to obtain ripple-free waveforms. The reference waveforms are the interfacial ones in Section III.

Fig. 7 shows the variation of the HH-case waveform in Fig. 3(b). In Fig. 7(a) and (d) are shown the deformations caused by the sharpest singularities of the spherical space waves, i.e., the singularities of the $\delta'(t)$ type and of the Hilbert-transformed $\mathcal{H}\delta'(t)$ type. These singularities are operationally defined by $\delta'(t) \otimes g(t) = g'(t)$ and $\mathcal{H}\delta'(t) \otimes g(t) = (-\pi t)^{-1} \otimes g'(t) = \partial_t(\mathcal{H}g(t))$, respectively, for a well-behaved function $g(t)$. The $\mathcal{H}\delta'(t)$ singularity can be inferred from the "logarithmic infinity" of the acoustical wave potential [7], [8]. To find out which singularity will dominantly or solely perturb the HH-case waveform, one can utilize the time-harmonic azimuthal far fields (which are of the TE type) in [12, eqs. (57) and (69)] derived for positive frequency, with the recognition of the (generalized) Fourier time transform relations $\mathfrak{F}^{\mathrm{i}}\{j\omega\} = \delta'(t)$ and $\mathfrak{F}^{\mathrm{i}}\{|\omega|\} = -\mathcal{H}\delta'(t)$. The asymmetric perturbation near $t = 47.2$ ns in Fig. 7(a) is due to the $\delta'(t)$ singularity, and the symmetric growth near 124.8 ns in Fig. 7(d) is due to the $\mathcal{H}\delta'(t)$ singularity. These effects are of first order, approximately proportional to z/ρ near the interface. The TM peaks (near 57.8 and 133.4 ns) are little affected by the offset. They almost overlap. This can be explained by the meridional far fields in [12, eqs. (56), (64), and (68)]; that is, further processing them, one can find out that the E field of the TM type is primarily in the meridional direction. Near the interface, therefore, the TM perturbation on the horizontal E field is not of first order.

The peaks in Fig. 7(b) characterize the "unguided" surface waves [induced by the spherical waves in the medium 2 shown in Fig. 7(d)], in the sense that a "guided" wave has a slower radial attenuation than the spherical wave. This unguided wave is also called the inhomogeneous (surface) wave [2, p. 109], [13]. For a point source, the unguided surface wave falls off as ρ^{-2} along the interface, an order faster than the spherical wave. In contrast, the surface wave guided by an interface (as the Rayleigh and Stoneley waves) or a slab (as the Love wave) falls off as $\rho^{-1/2}$ [1, Sec. 5.6], [6, Secs. 6.3 and 7.4.2].

In the $+z$ direction, the peaks in Fig. 7(b) exhibit a decay of z^{-1}, which is implied in the time-domain counterpart of the near-interface factor $\exp[ik_2\rho - (k_2^2 - k_1^2)^{1/2}(z + 2d_1)]$ in [2, p. 97] or a similar factor in [13]. Note that the exponential decay (in the frequency domain) is not invariantly transferred into the time domain. As regards the waveforms in Fig. 7(b), the z^{-1} decay implies that only the solid-line peaks are associated with the δ functions [i.e., $\delta(t_{\mathrm{h}2})$ and $\delta(t_{\mathrm{v}2})$ in (23)]. The dashed- and dotted-line peaks have finite magnitudes even when the source

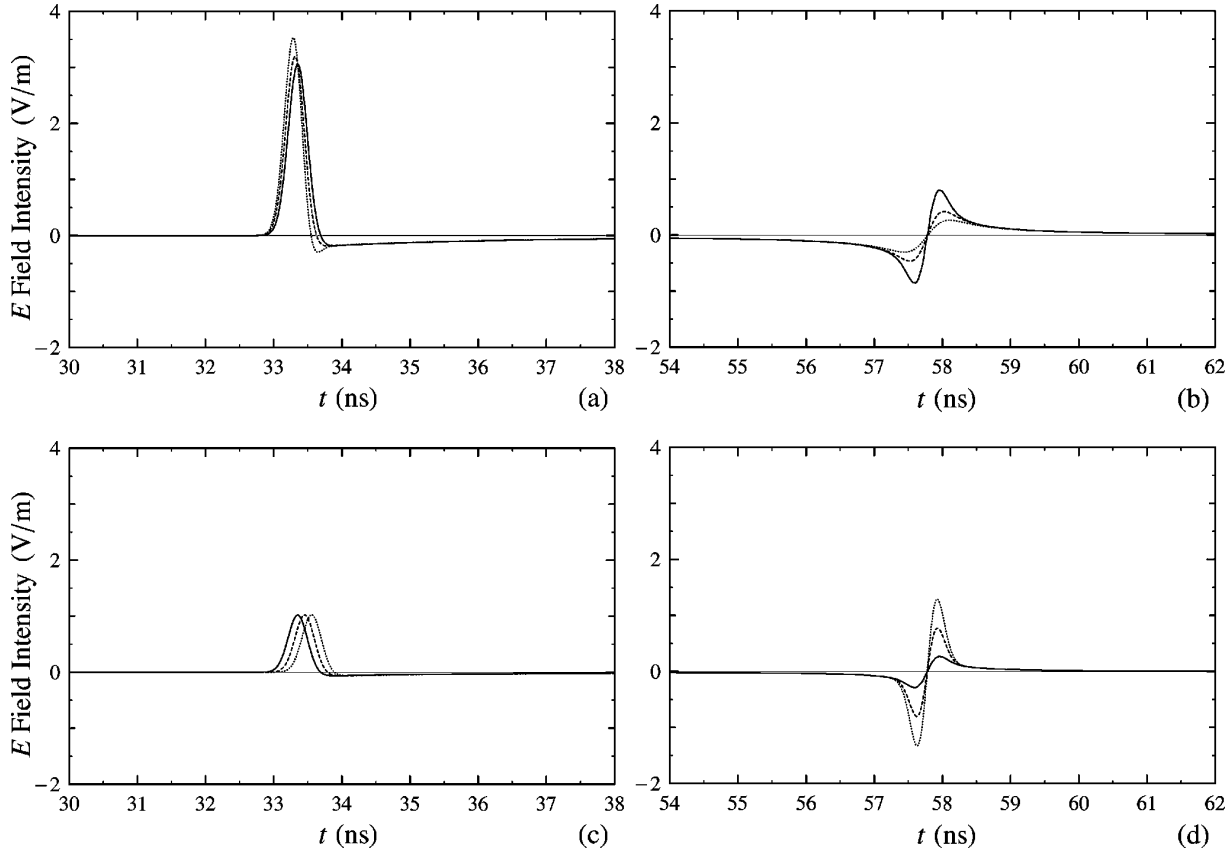

Fig. 9. The effects of the receiver's offset on the HV-case waveform of Fig. 5(a). (a) and (b) Solid, dashed, and dotted curves are for $z = 0^+$, 2, and 4 cm, respectively. (c) and (d) Solid, dashed, and dotted curves are for $z = 0^-$, -2, and -4 cm, respectively.

has an ideal waveform $\delta(t)$ instead of $\delta_T(t)$. In the time domain, the surface waves are singular only at the interface.

The dashed- and dotted-line peaks in Fig. 7(c) characterize the lateral head waves. The peaks just after $t = c_{\rm h1}^{-1} L^{\rm TE}$ (≈ 47.2 ns) pertain to the TE fronts and those just after $c_{\rm v1}^{-1} L^{\rm TM}$ (≈ 57.8 ns) pertain to the TM fronts. They travel most of their ways just within the medium 1, and then penetrate into the medium 2 at the critical angles, $\theta_{\rm c}^{\rm TE}$ and $\theta_{\rm c}^{\rm TM}$, respectively. They precede the spherical waves at $t = c_{\rm h2}^{-1}(\rho^2 + z^2)^{1/2}$ and $c_{\rm v2}^{-1}(\rho^2 + \chi_2^2 z^2)^{1/2}$ [the dashed- and dotted-line peaks in Fig. 7(d)] transmitted through the medium 2. The arrival times of the head waves are more affected by the offset than those of the spherical waves are.

Similar remarks can be made for the effects of the receiver's offset on the VV-case waveform, shown in Fig. 8 (calculated for the parameters used in Fig. 4). The variations of waveforms are similar to those of the HH-case TE waveforms in Fig. 7. For example, the asymmetric perturbation in Fig. 8(a) is due to the $\delta'(t)$ singularity, and the symmetric growth in Fig. 8(d) is due to the $\mathcal{H}\delta'(t)$ singularity. Discrimination is made between the cases of $z = 0^+$ and 0^-, since the vertical E field is discontinuous at the interface.

The effects of the receiver's offset on the HV-case waveform are shown in Fig. 9, for the parameters used in Fig. 5. The perturbations in Fig. 9(a) and (d) are both due to the $\delta'(t)$ singularities, as can be inferred from the time-harmonic formulas in [12, eqs. (56) and (68)] after simplification. The off-interface waveforms in Fig. 9(b) are smooth curves [as those in Figs. 7(b) and 8(b)], not as sharp as the interfacial transients of the $(-\pi t_{\rm v2})^{-1}$ singularity mentioned in Section III-C. The shifting peaks in Fig. 9(c) characterize the head wave, preceding the space-wave bursts in Fig. 9(d).

The VH case is similar to the HV case.

VI. Conclusion

The authors have described the procedures of time-domain analysis for the electromagnetic fields radiating along the horizontal interface between vertically uniaxial media. Employing and extending the interface scheme of [16], the solutions of the E fields have been obtained in exact explicit forms for the HH and VV cases. For the HV and VH cases, the leading impulse components have been extracted analytically, though the complete fields have to be treated numerically. The impulse components that lead the TE/TM waveforms are important in understanding the interfacial far fields of earliest TE/TM arrivals, since they are closely related with the lateral head waves. Whether or not in the far zone, the impulse components are of significance in their own right as prominent singularities in the transient waveforms. The H fields have been obtained using the procedures for the E fields.

The authors have also discussed the effects of the receiver's offset on the E field waveforms. The key features of the offset effects are: (i) the deformation of the interfacial singularities by the spherical-wave singularities; (ii) the attenuation of peaks of

the unguided surface waves; and (iii) the delayed (i.e., head-wave) arrival of the leading impulse components. In the case of the surface wave, a far-field component in the frequency domain does not imply a time-domain singularity, except at the interface.

There is no need to express the time-domain solutions in different forms depending on the relative values of the horizontal and vertical permittivities. Hence the procedures in this paper can be exploited for the electromagnetic problem in which the upper and lower media have different permeability (and permittivity) values, and for the acoustic case of the fluid–fluid interface. The procedures can also be utilized to derive or check some partial solutions of the acoustoelastic or purely elastic problems.

APPENDIX
CALCULATION OF $I(a) = (2/\pi)\int_0^{\pi/2} \cos^2\beta\,\mathrm{d}\beta/(a-\sin^2\beta)$

One can write $I(a)$ as

$$1-(a-1)\int_0^{\pi/2}\frac{\frac{2}{\pi}\,\mathrm{d}\beta}{a-\sin^2\beta} \tag{59}$$

for which it will be shown that

$$\int_0^{\pi/2}\frac{\frac{2}{\pi}\,\mathrm{d}\beta}{a-\sin^2\beta} = \frac{\operatorname{sgn} a}{[a(a-1)]^{1/2}} \quad (a<0 \text{ or } a>1) \tag{60a}$$

$$= 0 \qquad (0<a<1). \tag{60b}$$

The first case ($a<0$ or $a>1$) can be proven using a formula of [25, p. 185] concerning the integral $\int \mathrm{d}x/(a+b\sin^2 x)$ for $b/a > -1$. In the second case ($0<a<1$), the integrand is singular at $\beta = \sin^{-1} a^{1/2}$. The integral can be written as

$$\frac{\frac{2}{\pi}}{(1-a)^{1/2}}\int_0^{\pi/2}\left(\frac{\cos\beta}{a-\sin^2\beta}+\frac{-1}{(1-a)^{1/2}+\cos\beta}\right)\mathrm{d}\beta \tag{61}$$

in which the integral for the first integrand is evaluated in the sense of the Cauchy principal value

$$\int_0^1\frac{(-1)\,\mathrm{d}x}{(x-a^{1/2})(x+a^{1/2})} = \frac{1}{2\,a^{1/2}}\int_0^1\left(\frac{\mathrm{d}x}{x+a^{1/2}}-\frac{\mathrm{d}x}{x-a^{1/2}}\right)$$

$$= \frac{1}{2\,a^{1/2}}\ln\frac{1+a^{1/2}}{1-a^{1/2}} \tag{62}$$

employing the variable change $x=\sin\beta$. The integral for the second integrand yields

$$\frac{-1}{2\,a^{1/2}}\ln\frac{1+a^{1/2}}{1-a^{1/2}} \tag{63}$$

according to a formula concerning $\int \mathrm{d}x/(a+b\cos x)$ for $0<a<b$ [25, p. 180]. Hence, (61) becomes zero, validating the case (60b). Substituting (60) into (59) gives (16).

REFERENCES

[1] L. B. Felsen and N. Marcuvitz, *Radiation and Scattering of Waves*. New York: IEEE, 1994.

[2] W. C. Chew, *Waves and Fields in Inhomogeneous Media*. Piscataway, NJ: IEEE, 1995.

[3] A. T. de Hoop, "Pulsed electromagnetic radiation from a line source in a two-media configuration," *Radio Sci.*, vol. 14, pp. 253–268, Mar.–Apr. 1979.

[4] K. I. Nikoskinen, "Time-domain analysis of horizontal dipoles in front of planar dielectric interface," *IEEE Trans. Antennas Propag.*, vol. 38, pp. 1951–1957, Dec. 1990.

[5] B. J. Kooij, "The electromagnetic field emitted by a pulsed current point source above the interface of a nonperfectly conducting earth," *Radio Sci.*, vol. 31, pp. 1345–1360, Nov.–Dec. 1996.

[6] K. Aki and P. G. Richards, *Quantitative Seismology*, 2nd ed. Sausalito, CA: Univ. Sci. Books, 2002.

[7] R. Bortfeld, "Exact solution of the reflection and refraction of arbitrary spherical compressional waves at liquid-liquid interfaces and at solid-solid interfaces with equal shear velocities and equal densities," *Geophys. Prosp.*, vol. 10, pp. 35–67, Mar. 1962.

[8] D. H. Towne, "Pulse shapes of spherical waves reflected and refracted at a plane interface separating two homogeneous fluids," *J. Acoust. Soc. Amer.*, vol. 44, pp. 65–76, Jul. 1968.

[9] A. T. de Hoop and J. H. M. T. van der Hijden, "Seismic waves generated by an impulsive point source in a fluid/solid configuration with a plane boundary," *Geophysics*, vol. 50, pp. 1083–1090, Jul. 1985.

[10] D. Cassereau and D. Guyomar, "Reflection of an impulse spherical wave at a plane interface separating two fluids," *J. Acoust. Soc. Amer.*, vol. 92, pp. 1706–1720, Sep. 1992.

[11] D. Cheng, J. A. Kong, and L. Tsang, "Geophysical subsurface probing of a two-layered uniaxial medium with a horizontal magnetic dipole," *IEEE Trans. Antennas Propag.*, vol. AP-25, pp. 766–769, Nov. 1977.

[12] N. Engheta, C. H. Papas, and C. Elachi, "Radiation patterns of interfacial dipole antennas," *Radio Sci.*, vol. 17, pp. 1557–1566, Nov.–Dec. 1982.

[13] A. P. Annan, "Radio interferometry depth sounding: Part1—Theoretical discussion," *Geophysics*, vol. 38, pp. 557–580, Jun. 1973.

[14] B. van der Pol, "On discontinuous electromagnetic waves and the occurrence of a surface wave," *IEEE Trans. Antennas Propag.*, vol. 4, pp. 288–293, Jul. 1956.

[15] T. T. Wu and R. W. P. King, "Lateral electromagnetic pulses generated by a vertical dipole on the boundary between two dielectrics," *J. Appl. Phys.*, vol. 62, pp. 4345–4355, Dec. 1987.

[16] W.-S. Lee and S. Nam, "Transient interactions between tiny interfacial antennas on half-space lossless dielectric," *Radio Sci.*, vol. 34, pp. 1027–1041, Sep.–Oct. 1999.

[17] K. Li, Y. Lu, and W.-Y. Pan, "Exact formulas for the lateral electromagnetic pulses generated by a horizontal electric dipole in the interface of two dielectrics," *Progress In Electromagn. Res.*, vol. 55, pp. 249–283, 2005.

[18] H. Lamb, "On the propagation of tremors over the surface of an elastic solid," *Philos. Trans. R. Soc. London*, ser. A, vol. 203, pp. 1–42, 1904.

[19] C. L. Pekeris, "The seismic surface pulse," *Proc. Nat. Acad. Sci. USA*, vol. 41, pp. 469–480, Jul. 1955.

[20] C. H. Dix, "The method of Cagniard in seismic pulse problems," *Geophysics*, vol. 19, pp. 722–738, Oct. 1954.

[21] A. T. de Hoop, "A modification of Cagniard's method for solving seismic pulse problems," *Appl. Sci. Res.*, vol. B8, pp. 349–356, 1960.

[22] M. Abramowitz and I. A. Stegun, Eds., Handbook of Mathematical Functions Mineola, NY, Dover, 1972.

[23] J. H. M. T. van der Hijden, "Quantitative analysis of the pseudo-Rayleigh phenomenon," *J. Acoust. Soc. Amer.*, vol. 75, pp. 1041–1047, Apr. 1984.

[24] W.-S. Lee and S. Nam, "Derivation of the transient solution of the horizontal interfacial electric field generated by a tiny horizontal current source on a uniaxially anisotropic half-space dielectric," (in Korean) *J. Korea Electromagn. Eng. Soc.*, vol. 11, pp. 313–321, Feb. 2000.

[25] I. S. Gradshteyn and I. M. Ryzhik, *Table of Integrals, Series, and Products*, A. Jeffrey, Ed., 5th ed. San Diego, CA: Academic, 1994.

[26] A. Ben-Menahem and S. J. Singh, *Seismic Waves and Sources*, 2nd ed. Mineola, NY: Dover, 2000.

Won-seok Lihh (M'07) received the B.S., M.S., and Ph.D. degrees in electronics/electrical engineering from Seoul National University, Seoul, Korea, in 1993, 1995, and 2000, respectively.

He is currently with Global Communication Technology (GCT) Research, Inc., Seoul. His research interests include time-domain theory and analysis for wavefields, EM modeling for circuit components and packages, and CMOS circuit design for RF front-ends.

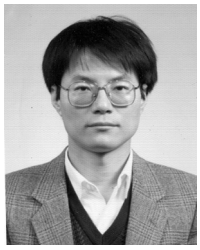

Sangwook Nam (S'87–M'88) received the B.S. degree from Seoul National University, Seoul, Korea, in 1981, the M.S. degree from Korea Advanced Institute of Science and Technology in 1983, and the Ph.D. degree from the University of Texas, Austin, in 1989, all in electronics/electrical engineering.

From 1983 to 1986, he was a researcher with Gold Star Central Research Laboratory, Seoul. Since 1990, he has been with Seoul National University, where he is currently a Professor in the School of Electrical Engineering. His research interests include analysis/design of EM structures, antennas, and microwave active/passive circuits.